SAPIENZA
UNIVERSITÀ DI ROMA

Faculty of Pharmacy and Medicine
Department of Molecular Medicine

PhD in Molecular Medicine - XXXI Cycle

Phenformin Inhibits Tumor Growth Through a Complex I-Independent Redox/Corepressor axis

Tutor:
Prof.Gianluca Canettieri

Candidate:
Simona Manni

Academic Year 2017-2018

SUMMARY

ABSTRACT

The antidiabetic drug phenformin displays potent anticancer activity in different tumors but its mechanism of action remains elusive. Using Shh Medulloblastoma as model, we show here that at the clinically relevant concentrations phenformin elicits a significant therapeutic effect through a redox-dependent, but complex I-independent mechanism. Phenformin inhibits mitochondrial glycerol-phosphate dehydrogenase (mGPD), a component of the glycerophosphate shuttle, and causes elevations of intracellular NADH content. Inhibition of mGPD mimics phenformin action and promotes an association between the corepressor CtBP2 and Gli1, thereby inhibiting Hh transcriptional output and tumor growth. Since ablation of CtBP2 abrogates the therapeutic effect of phenformin in mice, these data illustrate a biguanide-mediated redox/corepressor interplay, which may represent a relevant target for tumor therapy.

INTRODUCTION

The biguanides metformin and phenformin are antidiabetic drugs associated to well-established anticancer properties in preclinical and clinical settings (Pollak, 2013).

Metformin is the only biguanide currently approved for the treatment of type 2 diabetes and it is the most prescribed oral antidiabetic drug worldwide. Phenformin was prescribed for the treatment of diabetes until 1977 and then its use has been discontinued because of the more frequent occurrence of lactic acidosis (64 cases every 100.000) compared to metformin (6 cases every 100.000)(Berger, 1985). However, studies in the last years have documented a wider and more pronounced antitumor efficacy of phenformin compared to metformin, thus raising a renovated interest on this drug and its mechanism of action (Janzer et al., 2014; Rosilio et al., 2013; Shackelford et al., 2013).

How biguanides exert their therapeutic effect in diabetes and cancer has been the subject of intensive investigation and debate. The most accepted model links the effect of these drugs to their ability to inhibit the mitochondrial respiratory complex I, thereby inducing an imbalance of the intracellular redox and energetic states, associated with the increase of the NADH/NAD+ and AMP/ATP ratios, respectively (Foretz et al., 2014).

A key target activated by the increase of AMP/ATP ratio is the energy sensor AMPK, which has been linked to many of the downstream effects of biguanides in previous studies. However, the actual contribution of this kinase to the therapeutic response to these drugs has been the subject of conflicting results. It was initially proposed that the glucose-lowering effect of biguanides could be attributed to their ability to activate LKB1/AMPK, thus reducing the hepatic glucose production by turning off the transcriptional gluconeogenic program mediated by CRTC2-CREB (Shaw et al., 2005; Zhou et al., 2001). Later it has been demonstrated that the glucose-lowering effect of metformin is intact in mice lacking AMPK in the liver, thus raising concerns on the actual relevance of this kinase in the therapeutic response to metformin (Foretz et al., 2010; Miller et al., 2013).

A substantial amount of work has pointed at AMPK also as the key mediator of the direct anticancer properties of biguanides. This has been largely attributed to the ability of AMPK to inhibit mammalian Target of rapamycin (mTOR), by phosphorylating and activating the Tuberos Sclerosis complex 2 (TCS2), thereby inhibiting key processes such as protein synthesis, cell growth and viability (Shaw, 2009). In addition, biguanides have been found to inhibit mTOR activity independently of AMPK, by regulating RAG-GTPase (Kalender et al., 2010).

A major concern that has emerged in recent years is that the majority of the studies that support the above described mechanisms have been performed using supra-pharmacological, millimolar doses of biguanides, while the plasma concentrations reached in patients after oral assumption are 10 to 100 times lower, within the low micromolar range (He and Wondisford, 2015). Inhibition of complex I, for instance, requires elevated doses of metformin, around 1-5 mM in *in vitro* biochemical studies (El-Mir et al., 2000). This suggests that alternative targets and cellular events other than inhibition of complex I, and the consequent drop in cellular energy charge, may contribute to the antitumor effects of biguanides at the micromolar doses. However, these mechanisms are still poorly understood.

Shh Medulloblastoma (Shh MB) is a pediatric brain tumor characterized by an aberrant activation of the developmental Sonic Hedgehog (Shh) signaling. This pathway regulates key steps during embryonic and postnatal development and stem cell fate in the adulthood (Briscoe and Therond, 2013).

The Shh signaling cascade starts with the binding of the Shh ligand to the receptor Patched (Ptch), leading to the de-repression of the transmembrane transducer Smoothened (Smo). This triggers a signaling cascade involving the cytoplasmic regulator Suppressor of Fused (SuFu) and terminating with the activation of the transcription unit: Gli1, Gli2 and Gli3. Gli1 is a target of the Hh signaling and a powerful transcription factor and oncogene, upregulated in Shh MB.

Mutations of genes encoding pathway components (*Ptch, Smo, SuFu, Gli2*) and causing an upregulation of the signaling are typically found in the Shh Medulloblastoma subgroup. Hence, Hh inhibitors represent an ideal class of drugs for this type of malignancy. The only FDA-approved compound, the Smo antagonist Vismodegib, has shown limited efficacy in patients due to the occurrence of novel Smo mutations or to post-receptor mutations. For this reason, other strategies are being conceived, mainly focused on the identification of Hh inhibitors acting at post-receptor level (Di Magno et al., 2015), ideally targeting Gli1 (Infante et al., 2015). In this regard, our group and others have recently observed that the energy sensor AMPK turns off the canonical Hh signaling by phosphorylating and inhibiting Gli1 (Di Magno et al., 2016; Li et al., 2015). Therefore, this observation suggested that the pharmacological activation of AMPK could represent a promising avenue to inhibit Hh signaling and to counteract Hh-dependent tumors.

Given the reported ability of biguanides to promote AMPK function, in the present work we have investigated the ability of these drugs to provide therapeutic benefit when used at the clinically relevant concentrations in preclinical models of Shh Medulloblastoma.

Unexpectedly, we found that phenformin elicits a robust anticancer effect that is independent of complex I-AMPK axis, but dependent on a previously uncharacterized glycerophosphate-corepressor interplay.

RESULTS

Clinical doses of phenformin inhibits MB growth and Hh signaling

We tested the effect of metformin and phenformin on the growth of Med1-MB cells, a tumor cell line where the developmental Hedgehog signaling is aberrantly activated. These cells were obtained from a medulloblastoma originated in $Ptch^{+/-}$ mouse (Hayden Gephart et al., 2013; Tang et al., 2014) carrying the monoallelic inactivation of the inhibitory receptor *Patched1* gene, which leads to the constitutive activation of Hh pathway (Goodrich et al., 1997). The growth of these cells depends on Hh signaling and can be inhibited by antagonists of the pathway. Both biguanides were tested within the micromolar range (1-100 μM), in media containing 5.5 mM and 0.75 mM glucose, corresponding to the average physiological plasma fasting and estimated cancer tissue glucose concentrations, respectively (Birsoy et al., 2014). To prevent glucose depletion, media was replaced every 6 hours and the glucose concentration was monitored at the end of each experiment. Exposure of Med1-MB cells to metformin did not cause any significant change of tumor growth in both glucose regimens (Figure 1A, top) at any of the concentrations tested, likely reflecting the low levels of metformin OCT1 and OCT3 transporters in these cells, as observed in other tumors (Jackson et al., 2017; Segal et al., 2011). Conversely, the more permeable phenformin induced a significant inhibition of cell growth starting form doses as low as 1-5 μM at both glucose concentrations, being the effect stronger at 0.75 mM glucose (Figure 1A, bottom).

A

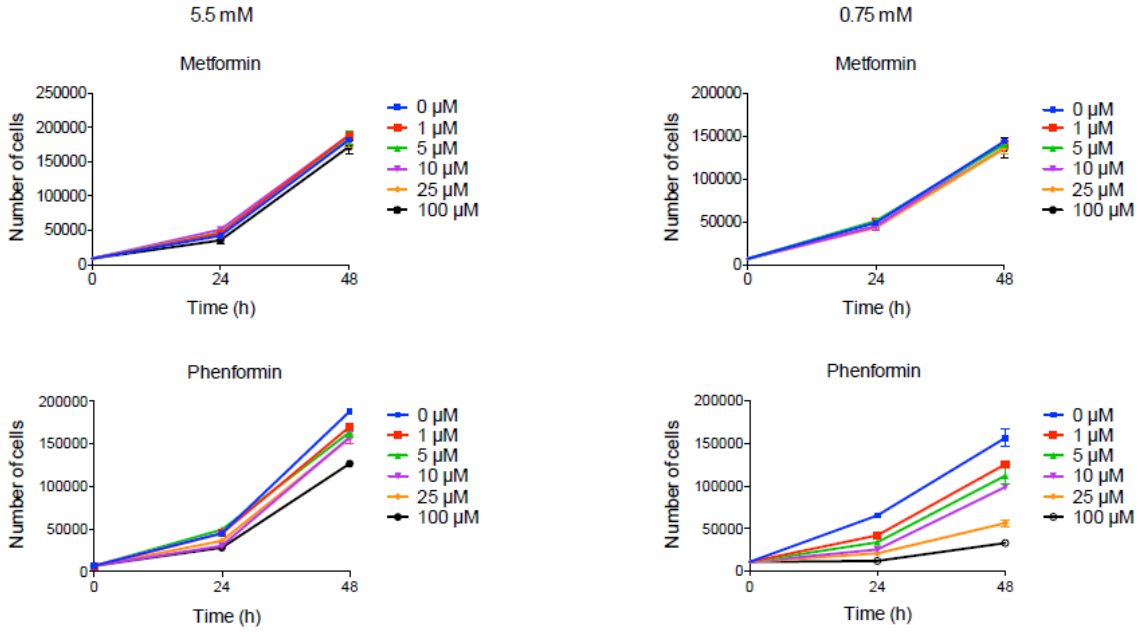

Figure 1. A, Med1-MB cells were treated with metformin (up) or phenformin (bottom) at different concentrations, as indicated in the Figure, in media containing 5.5mM (left) or 0.75mM (right) glucose. Data are representative of three independent experiments, each performed in triplicate.

Similar data were observed in primary cultures of Shh MB, obtained from Math1-CRE; Ptch1$^{loxP/loxP}$ mice, carrying the homozygous deletion of Ptch1 gene in Math1-expressing granule cell progenitors, which causes MB with complete penetrance (Yang et al., 2008). Micromolar doses of phenformin caused a reduction of tumor cell growth also in this model, confirming the inhibitory effect in cell culture (Figure 2A).

A

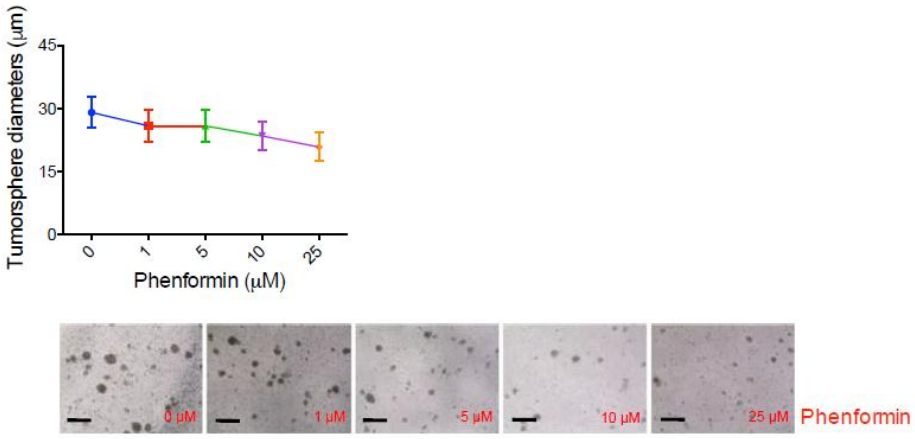

Figure 2. A, Phenformin treatment impairs the ability of primary medulloblastoma cells to form tumorspheres. (up) Average diameter of tumorspheres treated with vehicle (DMEM) or phenformin as indicated in the Figure. Bottom, representative images of tumorspheres as described above. Scale bar = 100 μm.

Once established the antitumor efficacy of phenformin on Shh MB growth *in vitro*, we sought to determine the most appropriate concentration of usage, by measuring the plasma levels of the drug in mice (Figure 3A). We first injected increasing amounts (1-12.5mg/Kg) of phenformin in the tail vein and measured the blood concentrations after 30 minutes and 1 hour. As shown in Figure 3B the highest concentration detected, reached by injecting 12.5 mg/Kg of drug, did not go beyond 5 μM, while higher doses were not tolerated by the animals.

We also evaluated the average circulating concentration of phenformin reached in a cohort of mice treated with 300 mg/Kg/day in the drinking water, corresponding to the maximum administrable dose (Appleyard et al., 2012; Huang et al., 2008). Under these conditions, the plasma concentration of the drug reached after 10 days of treatment was about 1.4 μM (Figure 3C), which corresponds to the average plasma concentration reached in diabetic patients that were treated with phenformin (Nattrass et al., 1980). Therefore, we established 1-5 μM as the proper therapeutic range of phenformin concentrations to be used in the subsequent analyses.

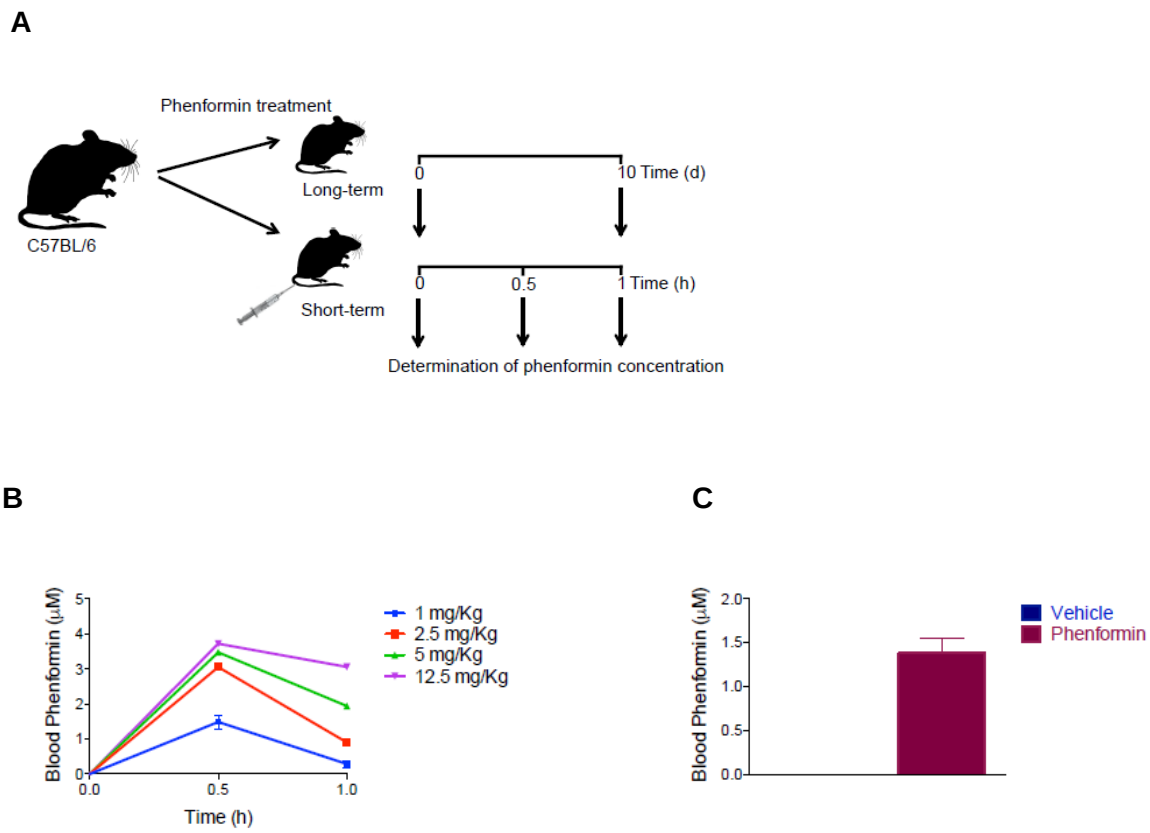

Figure 3. A, Experimental scheme of phenformin treatment on C57BL/6 mice. Mice were treated with phenformin (300mg/Kg/day) via ad libitum feeding and samples collected after 10 days (long-term treatment). For short-term treatments, mice were administered with phenformin by tail vein injection, and samples were collected at 30 minutes and 1 hour for subsequent analysis. **B**, HPLC analysis of circulating blood plasma phenformin from C57BL/6 mice (n=4) after tail vein injection, at the indicated concentrations. **C**, HPLC analysis of phenformin (µM) in circulating blood plasma from C57BL/6 mice (n=6). Blood plasma was analyzed after 10 days of ad libitum administration of vehicle (water) or phenformin (300mg/Kg/day) *per os*.

We grafted tumor cells from freshly isolated Shh MB, obtained from Math1-CRE; Ptch1$^{loxP/loxP}$ mice described above, into the flanks of immunodeficient athymic nude mice. When the average tumor volume reached 100 mm^3, mice were treated with 300 mg/Kg/day phenformin *per os* (Appleyard et al., 2012) and the growth of the tumor masses was measured every 3 days.

As shown in Figure 4A in phenformin-treated mice tumors grew significantly slower compared to controls and, at the end of the treatment, showed a significant decrease in tumor size and weight and of cellular proliferation, as assessed by Ki67 staining.

We also measured the overall survival in a cohort of Math1-CRE; Ptch1$^{loxP/loxP}$ mice upon oral administration of phenformin. While control littermates had a median survival of 49 days after the beginning of the treatment, the survival of mice treated with phenformin was increased by almost 40% (68 days after treatment), indicating the preclinical efficacy of this drug on intracranial, spontaneously generated tumors (Figure 4B).

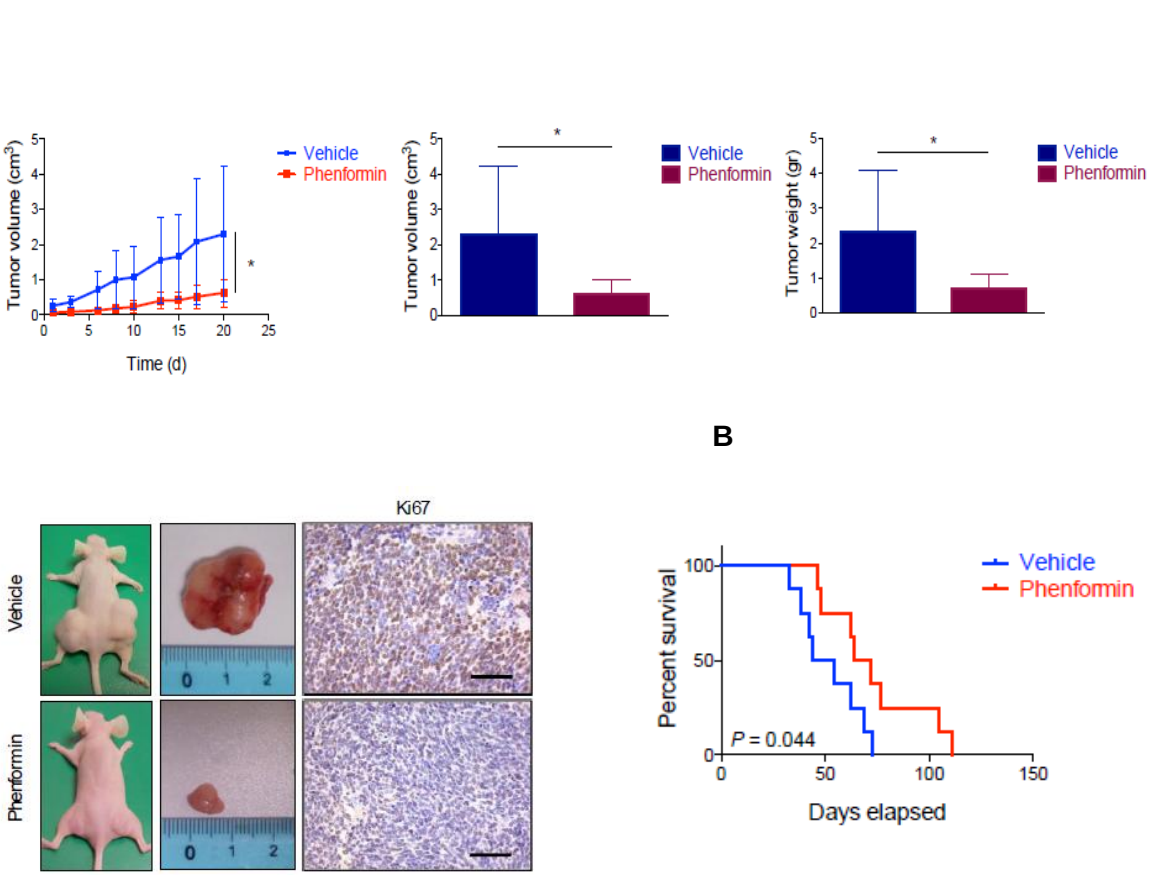

Figure 4. A, (Top, left) growth curves of allograft tumors after injection of primary medulloblastoma cells from Math1-CRE; Ptch1$^{loxP/loxP}$ mice in CD1-nude mice treated with vehicle (water) or phenformin (300 mg/kg/day) ad libitum *per os*. Tumor volume (cm^3) was measured at the indicated times. Tumor volume (top, middle) and weight (top right) were measured at the end of the experiment. Bottom, representative images of allografted mice and isolated tumors at the end of the experiment. Ki67 staining in excised Med1-MB allograft tumor tissues in phenformin-treated mice or untreated group is shown. n=5 mice per treatment group. Scale bar = 150μm. **B**, Kaplan-Meier curve for Math1-CRE; Ptch1$^{loxP/loxP}$ mice treated with vehicle (water) (n=8) or phenformin (n=8). p = 0.044 as determined by log-rank test.

Phenformin inhibits Hedgehog signaling independently of the energy sensing machinery

Since a key tumorigenic driver of Shh MB subgroup is an aberrant function of the Hedgehog (Hh) signaling, we wondered whether the observed inhibitory effect could be related to the ability of phenformin to interfere with this developmental pathway. To this end, we measured the mRNA levels of Gli1, a well-established Hh target gene, in primary cultures of mouse Shh MB and in Med1-MB cells and found that they were reduced by therapeutic concentrations of phenformin (Figure 5A).

A

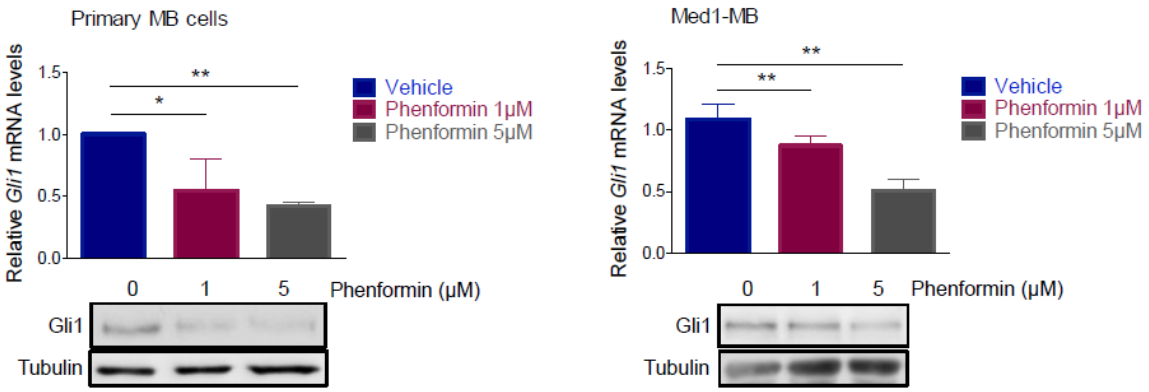

Figure 5. A, Relative *Gli1* mRNA expression levels in primary tumorspheres derived from Math1-CRE; Ptch1$^{loxP/loxP}$ mice (left) and Med1-MB cells (right) as determined by qPCR. Cells were treated with vehicle (DMEM) or phenformin at the indicated concentrations in media containing 0.75mM glucose, for 48 hours. Gli1 protein levels are shown. Tubulin was used as a control for equivalent lane loading.

We also tested the drug on DAOY cells, an Hh-responsive MB cell line (Gotschel et al., 2013). Treatment of these cells with the Smo agonist SAG (Gotschel et al., 2013) caused an increase of Gli1 that was robustly prevented by the biguanide (Figure 6A).

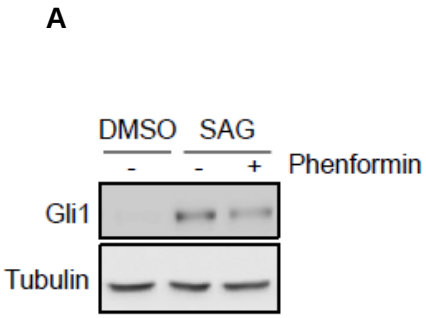

Figure 6. A, Whole cells lysates from DAOY cells treated with SAG or DMSO, and phenformin (5μM) for 48 hours. Gli1 levels were analyzed by western blot. Tubulin was used as loading control.

Phenformin also inhibited Ptch1, Cyclin D2, Cyclin D1, Cyclin A, Cyclin E and increased p21 levels indicating the ability of this drug to antagonize Hedgehog signaling and its cell cycle-related targets (Che et al., 2013; Kenney and Rowitch, 2000; Plaisant et al., 2011) at the clinically relevant doses (Figure 7A).

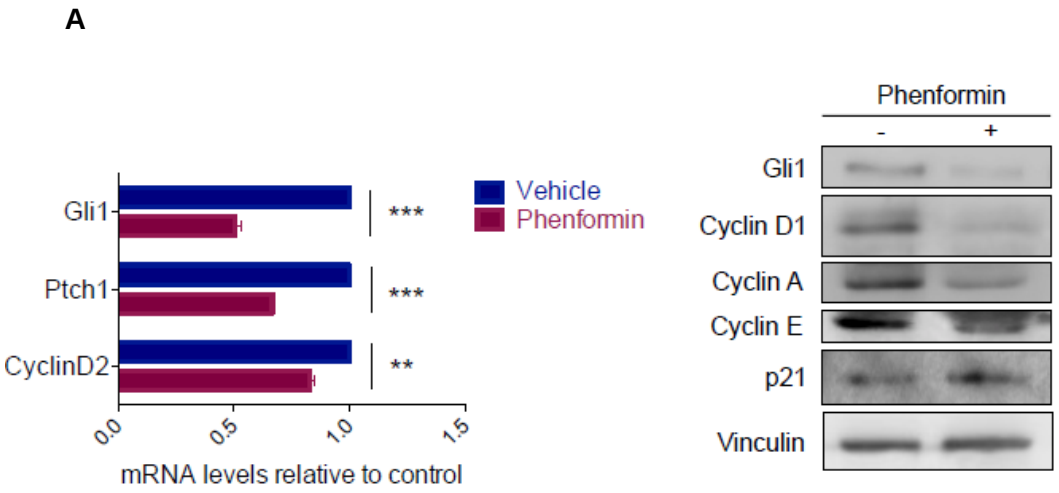

Figure 7. A, Left, relative expression of *Gli1*, *Ptch1* and *CyclinD2* mRNA in vehicle (DMEM) or phenformin (5μM) treated primary tumorspheres from Math1-CRE; Ptch1$^{loxP/loxP}$ mice, as evaluated by qPCR. Expression levels were normalized to *L32* mRNA levels and represented as fold change relative to control (vehicle) sample. Right, western blot analysis of the indicated targets in Med1-MB cells after 48 hours of treatment with phenformin (5μM) or vehicle (DMEM). Vinculin expression was used to determine equivalent lane loading.

To establish at what level of the Hh pathway phenformin exerts its action, we knocked down the cytoplasmic inhibitor SuFu from DAOY cells. As expected (Gruber et al., 2018),

deletion of SuFu caused an upregulation of Hh transcriptional activity that was independent of Smo receptor, as demonstrated by the increased levels of Gli1 that were not suppressed by the Smo inhibitor KAAD. Conversely, phenformin treatment caused a significant inhibition of Gli1 protein and mRNA levels in SuFu-deficient cells, thus indicating that the drug acts downstream of Smo, likely by affecting Gli activity (Figure 8A).

A

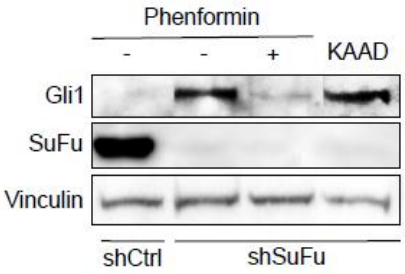

Figure 8. A, Western blot analysis of DAOY cells stably transduced with control (shCtrl) or SuFu-specific (shSuFu) shRNAs and treated with phenformin (5μM) or KAAD (1μM) for 48 hours. Gli1 and SuFu protein levels are shown. Vinculin was used as loading control.

Since the canonical Hh signaling is inhibited by AMPK via Gli1 phosphorylation, and given the reported ability of phenformin to activate this kinase, we wondered whether under our experimental conditions the observed effects could be mediated by AMPK.

At the therapeutic doses, however, we could not detect any change of AMPK phosphorylation at T172, a marker of AMPK activation, at both early (1 hour) and late (48 hours) time points, whereas we could detect AMPK phosphorylation at millimolar doses (Figure 9A). Furthermore, as phenformin maintained its ability to reduce proliferation in Shh-MB cells depleted of AMPKα1, the only AMPK catalytic isoform expressed in these cells (Figure 9B, 9C, 9D), we ruled out the involvement of this kinase in the observed effect.

In most cases, the antitumor properties of biguanides have been attributed to their ability to directly or indirectly inhibit mTOR, a kinase often upregulated in tumors that also

modulates Gli activity (Wang et al., 2012). Thus, we investigated the involvement of mTOR by analyzing the phosphorylation levels of its well-known substrate 4EBP. Also in this case, phosphorylation of this protein was not affected by phenformin at the micromolar concentrations, while it was inhibited at 1 mM (Figure 9A), leading us to conclude that under therapeutic conditions, phenformin exerts its antitumor effect through mTOR-independent mechanisms.

Finally, since it was found that biguanides affect PKA activity in the liver by depleting AMP and thus cAMP levels (Miller et al., 2013), we also tested the levels of phosphorylated CREB, a PKA target that may play a role in tumorigenesis (Steven and Seliger, 2016). As shown in Figure 2E, phenformin did not modify P-CREB at any of the concentrations tested.

Therefore, these observations indicated that at the established therapeutic concentrations phenformin does not affect any of the previously characterized AMP-dependent targets.

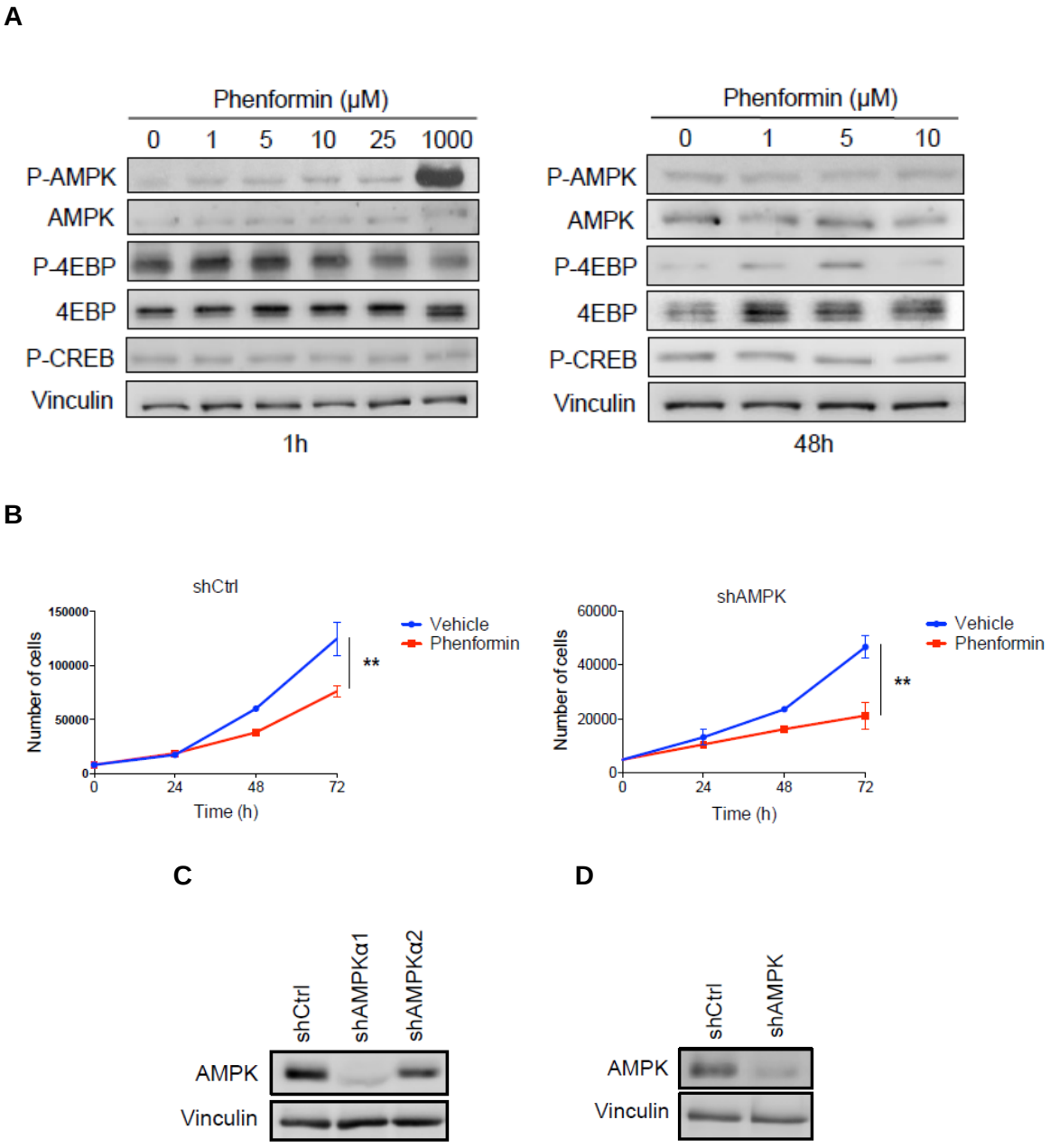

Figure 9. A, Med1-MB cells were treated with the indicated increasing concentrations of phenformin at early (1 hour) and late (48 hours) time points. Lysates were analyzed by immunoblot for the indicated proteins. **B**, Proliferation assay on Med1-MB cells expressing control (shCtrl) or AMPKα1-specific (shAMPK) shRNAs treated with phenformin (5μM) for the indicated time points. **C**, Whole cell lysates from Med1-MB cells transduced with lentiviruses expressing shControl (shCtrl), AMPKα1-specific or AMPKα2-specific shRNAs were analyzed by immunoblot using the indicated antibodies. Vinculin as loading control. **D,** Western blot analysis of cell lysates from Figure B, using the indicated antibodies. Vinculin as loading control.

The antitumor effect of phenformin is mediated by mGPD-dependent changes of the redox state

Since biguanides are believed to exert most of their actions by inhibiting mitochondrial respiratory complex I (Dykens et al., 2008; El-Mir et al., 2000; Owen et al., 2000) we wondered whether under our experimental conditions the activity of this complex is affected by the drug. Inhibition of the respiratory complex I causes a decrease of the oxidative phosphorylation and a consequent reduction of the oxygen consumption and energy balance, with a parallel increase of the redox state, due to the lack of oxidation of the reducing equivalents.

In contrast with this scenario, cells treated with therapeutic doses of phenformin showed an oxygen consumption rate (OCR) that was not significantly altered (Figure 10A), whereas it was strongly inhibited by the standard complex I inhibitor rotenone or by 1 mM phenformin (Figure 10B).

A **B**

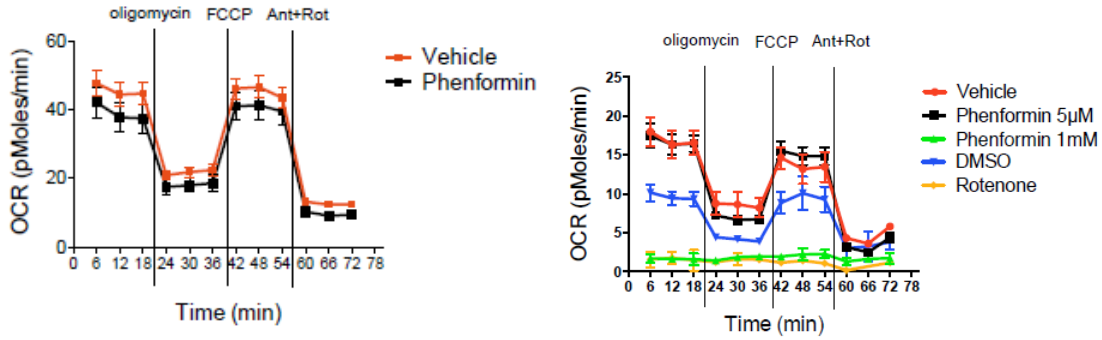

Figure 10. A, OCR in Med1-MB cells treated with phenformin (5μM, 6 hours) in media containing 0.75 mM glucose. **B**, Med1-MB cells were analyzed for oxygen consumption after treatment with phenformin (5μM or 1mM) or rotenone (1μM) for 6 hours. The oxygen consumption trace is shown.

Consistently, the ATP content was not modified by phenformin, while it was significantly reduced by rotenone (Figure 11A).

By contrast, the lactate/pyruvate ratio, and the total NADH content were significantly increased in phenformin-treated cells, documenting an increase of the intracellular redox state (Figure 11B, 11C).

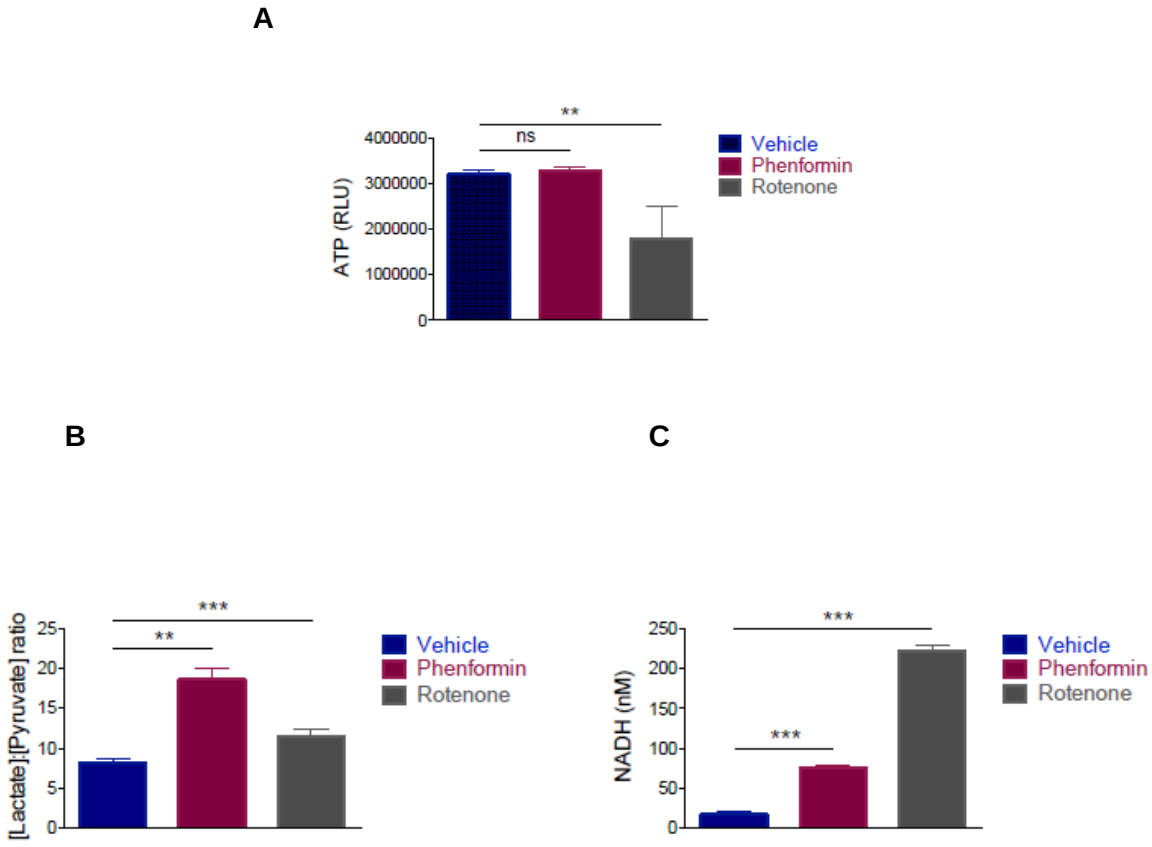

Figure 11. ATP (**A**) L-lactate (**B**) and NADH content (**C**) were determined in Med1-MB cells following treatment with phenformin (5μM) and rotenone (1μM) for 6 hours. ATP content is expressed as relative luminescence units (RLU), L-lactate production as the Lactate:Pyruvate ratio.

Similar alterations were found in mice, in allografted or spontaneously generated Shh MB tumors, chronically or acutely treated with phenformin, respectively. In these samples, the lactate/pyruvate ratio and NADH content were significantly increased, while the ATP levels, as well as phosphorylated AMPK, were unchanged (Figure 12A, B, C), further indicating the exclusive modification of the redox state in phenformin-treated tumors *in vivo*.

A

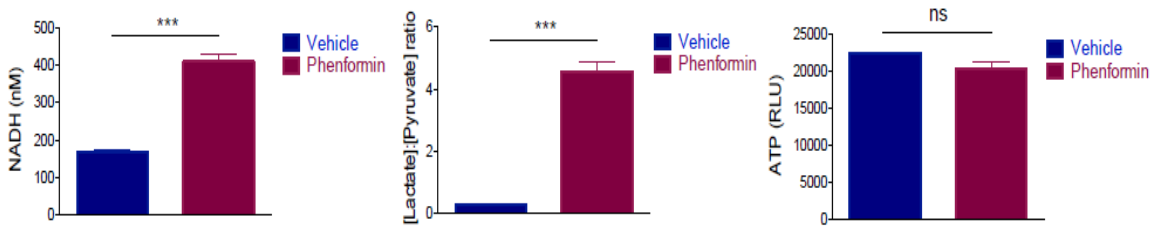

B

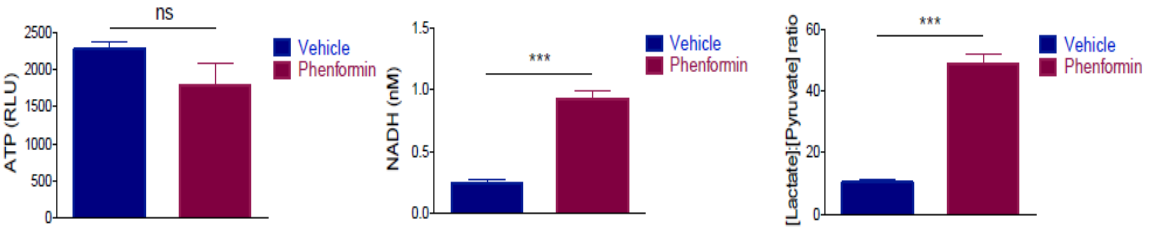

C

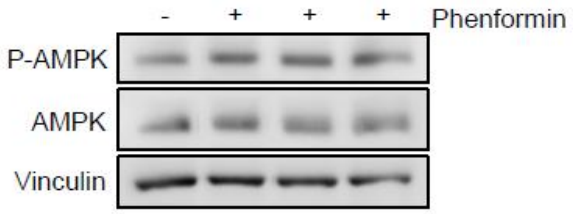

Figure 12. A, Short-term phenformin treatment (12.5mg/Kg, i.v.) increases NADH and lactate production in medulloblastoma tissues from Math1-CRE; Ptch1$^{loxP/loxP}$ mice, but has no effect on ATP content. **B**, Long-term phenformin treatment (300mg/Kg/day, *per os*) causes an increase of NADH content and L-lactate production in allografted tumors (from Figure 4A), measured at the end of the experiment, with no significant effect on ATP content. **C**, Western blot analysis of medulloblastoma tissues as described in Figure 12 A, showing the phosphorylation levels of AMPK following i.v. injection of saline (0.9%) or phenformin (12.5 mg/Kg). Each lane represents an independent tumor.

Collectively, these observations suggest that the antitumor properties of therapeutic concentrations of phenformin are independent of complex I and are mediated by an alternative target, able to solely alter the redox balance. In this regard, it was found that biguanides non-competitively inhibit the mitochondrial glycerophosphate dehydrogenase

(mGPD) enzyme, a component of the glycerophosphate shuttle, leading to an increase of the redox state, accumulation of lactate, and suppression of hepatic gluconeogenesis (Madiraju et al., 2014).

To address the possibility that a similar mechanism could support our observations in tumor cells, we analyzed the energy and redox balance of Shh MB cells upon lentiviral knockdown of mGPD. As shown in Figure 13A and 13B, ablation of mGPD caused a significant increase of lactate/pyruvate ratio and NADH, indicating that mGPD deficiency mimics phenformin effect on the redox balance in tumor cells.

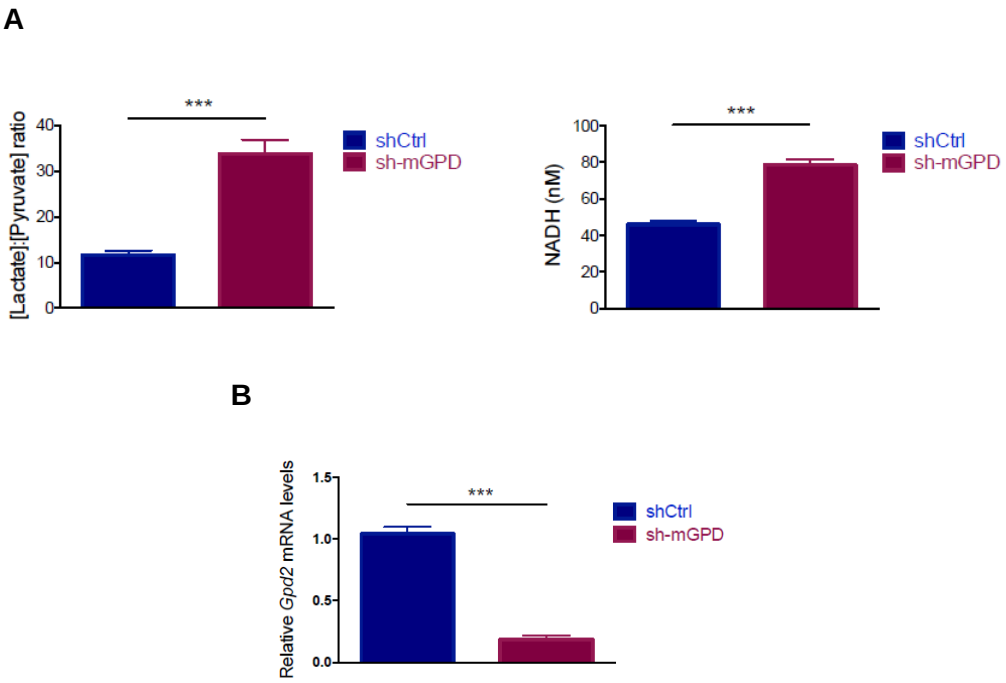

Figure 13. A, Measurement of L-lactate production (left) and NADH content (right) in shControl (shCtrl) and sh-mGPD expressing Med1-MB cells. **B,** Relative *mGPD* mRNA levels from Med1-MB cells expressing control or mGPD-specific shRNAs. Results were normalized on *L32* mRNA levels.

In keeping with this finding, ablation of mGPD, but not of the cytoplasmic GPD (cGPD), caused a significant decrease of Med1-MB cell proliferation (Figure 14A, B) and prevented the inhibitory effect of phenformin on tumor growth, demonstrating the requirement of this enzyme for tumor growth and for the therapeutic effect of phenformin.

A **B**

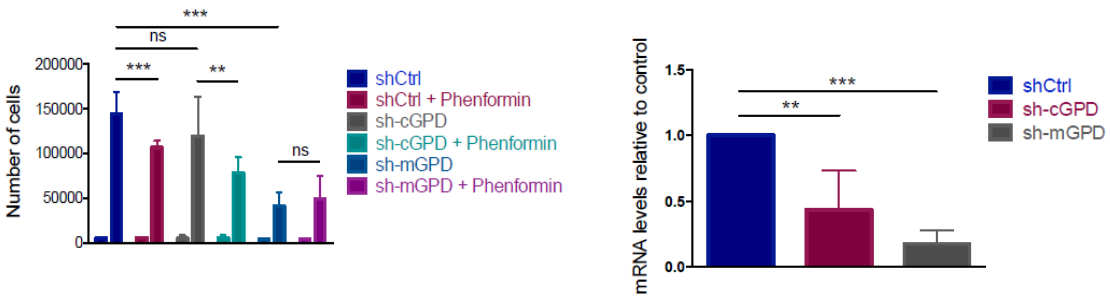

Figure 14. A, Proliferation assay on Med1-MB cells expressing shControl (shCtrl) or cGPD and mGPD-specific shRNAs and treated with phenformin (5μM) for 48 hours. **B**, c*GPD* and *mGPD* mRNA levels from Med1-MB cells expressing control or cGPD or mGPD-specific shRNAs. mRNA levels were normalized on *L32* mRNA, and results are expressed as fold induction relative to control sample.

Furthermore, both mRNA and protein levels of Gli1 were reduced upon knockdown of mGPD and the lack of this enzyme prevented further inhibition of phenformin on Hh-dependent gene expression (Figure 15 A, B), thus indicating that mGPD is a key mediator of the inhibitory effect of phenformin on the Hh signaling.

A

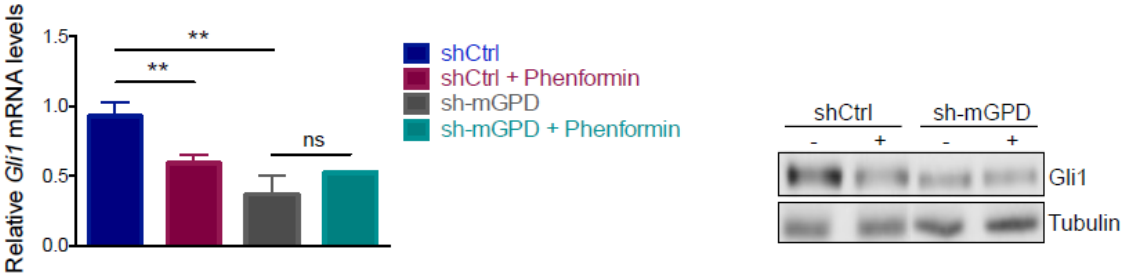

B

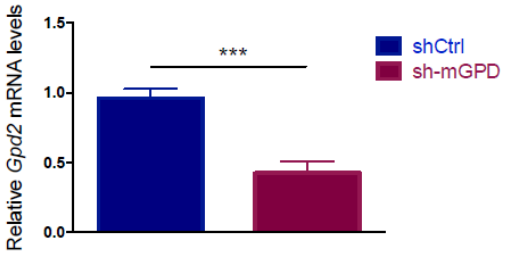

Figure 15. A, Expression of *Gli1* mRNA (left) and Gli1 protein levels (right) in vehicle (DMEM) or phenformin (5μM) treated Med1-MB cells expressing shControl (shCtrl) or sh-mGPD as determined by qPCR and western blot assays. Expression levels were normalized to *L32* mRNA levels, and tubulin levels are shown as control. **B**, Relative *mGPD* mRNA levels as in 15A).

Of note, treatment of MB cells with a selective mGPD antagonist, iGP-1 (Orr et al., 2014), resulted in a significant inhibition of tumor growth and Hh signaling (Figure16A), demonstrating that pharmacological targeting of mGPD mimics the biguanide effect.

A

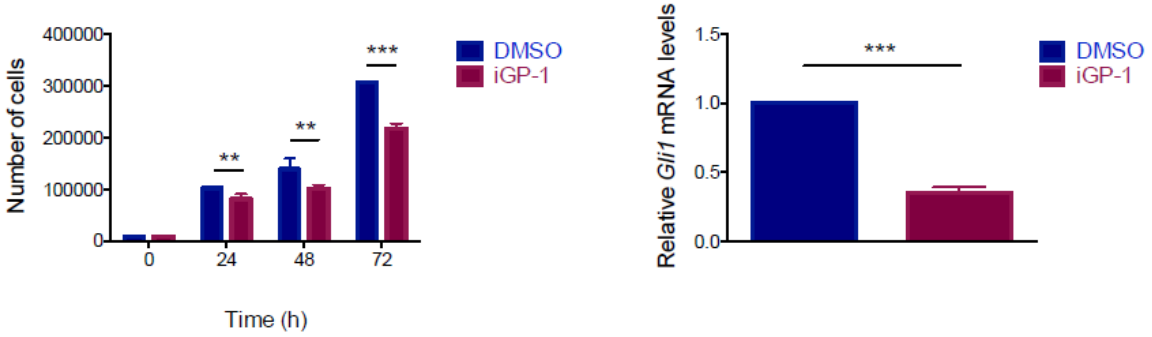

Figure 16. A, (Left) Proliferation assay on Med1-MB cells treated with vehicle (DMSO) or iGP-1 (1mM) for the indicated time points. (Right) qPCR of *Gli1* gene in Med1-MB cells collected at the end of the experiment (72 hours). mRNA levels were normalized to the expression of *L32*.

The NADH-dependent transcriptional corepressor CtBP2 mediates phenformin-induced Hh inhibition

Having found that mGPD mediates the phenformin effects by inducing accumulation of NADH, we wondered how this redox imbalance could be coupled to inhibition of Hh-dependent gene expression and tumor growth.

Since phenformin inhibits Hh-mediated transcription downstream of SuFu, we reasoned that a corepressor with the ability to sense the NADH levels and to inhibit Hh signaling could mediate the observed effect, possibly by associating with Gli.

We hypothesized that the C-terminal Binding Proteins (CtBP1 and CtBP2) could be involved in this mechanism since they have the ability to sense changes of NADH levels and to respond to their increase by associating with specific partners at the promoter levels, bringing about transcriptional repression (Chinnadurai, 2002).

In coimmunoprecipitation assays we observed that Gli1 binds to CtBP2, but not CtBP1 in Med1-MB cells (Figure 17 A).

Conversely, CtBP2 did not associate with Gli2 and Gli3, the other two Hh-regulated transcription factors (Figure 17 B).

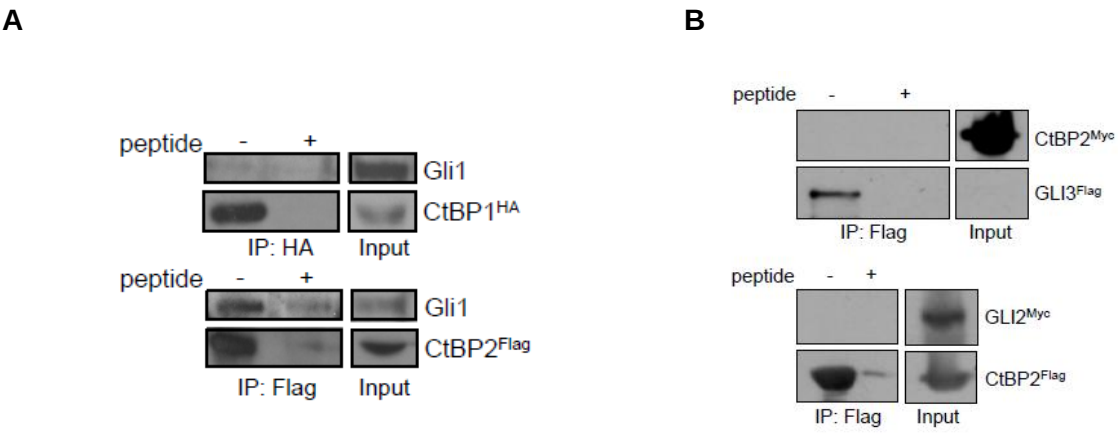

Figure 17. A, Immunoprecipitation assay on Med1-MB cells transiently transfected with HA-tagged CtBP1 or Flag-tagged CtBP2 plasmids. Lysates were immunoprecipitated with Flag or HA antibodies and western blot analysis was performed. Coimmunoprecipitated endogenous Gli1 protein levels are shown. Antibodies saturated with Flag peptide and HA peptide before IP were used as negative control. **B**, Immunoprecipitation assay on Med1-MB cells transiently transfected with Flag-tagged GLI3 and Myc-tagged CtBP2 or Flag-tagged CtBP2 and Myc-tagged GLI2 plasmids. Lysates were immunoprecipitated with Flag antibody and western blot analysis was performed. Flag peptide was used as negative control.

Phenformin treatment led to a time-dependent increase of the association between endogenous Gli1 and CtBP2 (Figure 18 A), as well as to increased CtBP2 recruitment over the Gli target gene *Ptch1* (Figure 18 B), indicating a drug-induced complex formation at the chromatin level.

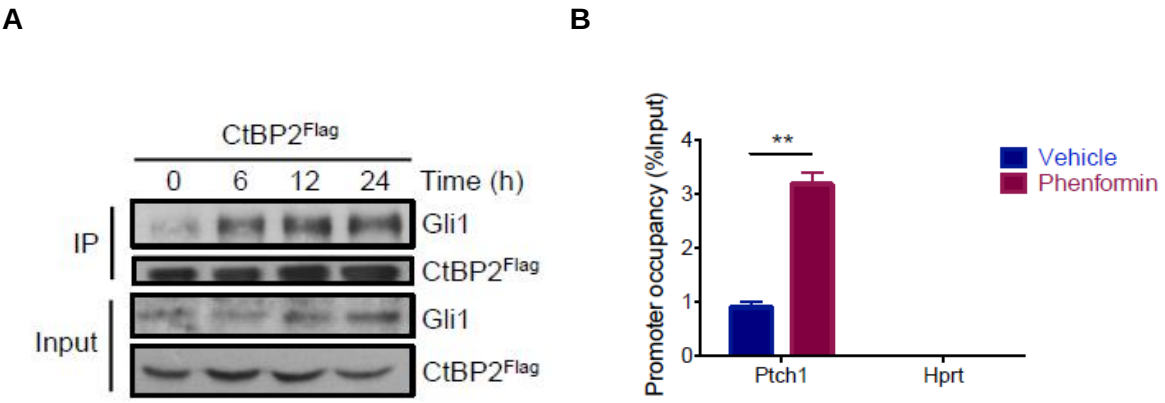

Figure 18. A, Med1-MB cells were transfected with Flag-tagged CtBP2 and treated with phenformin (5μM) for the indicated times. Cellular extracts were immunoprecipitated with Flag antibody and analyzed by western blot. Endogenous Gli1 protein levels are shown. **B**, Chromatin immunoprecipitation (ChIP) assay on Med1-MB cells treated with vehicle (DMEM) or phenformin (5μM) for 6 hours. Immunoprecipitation was performed with a CtBP2-specific antibody, and fold enrichment over IgG control was determined by qPCR analysis with primers encompassing *Ptch1* promoter. *Hprt* was used as negative control.

Supporting the specific ability of CtBP2 to limit Hedgehog activity at a downstream level, ectopic expression of CtBP2 reduced Gli1 activity on a Gli-responsive reporter and this effect was abrogated by siRNA-mediated knockdown of Gli1 (Figure 19 A).

A

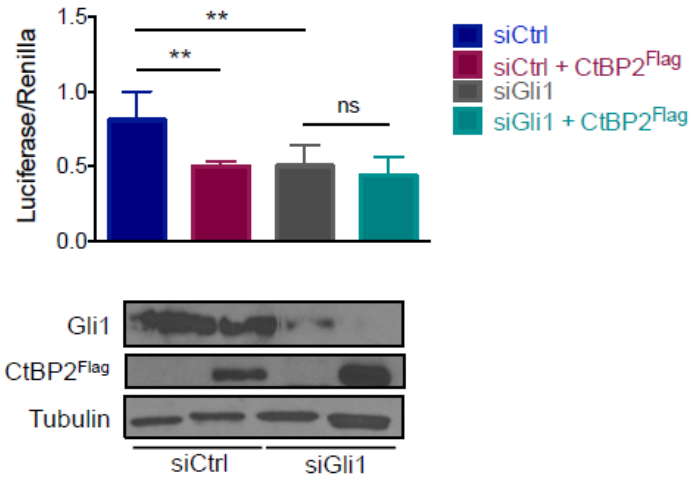

Figure 19. A, Effects of CtBP2 overexpression on Gli1 transcriptional activity in Med1-MB cells expressing siControl (siCtrl) or Gli1-specific siRNA, evaluated as Luciferase on Renilla activity.

To prove the functional connection of CtBP2 with mGPD we performed double lentiviral-mediated knockdown in Med1-MB cells. As shown in Figure 20 A and 20 B, ablation of mGPD caused a significant inhibition of cell growth and Hh signaling that was prevented in CtBP2 deficient cells, indicating the requirement of the redox sensor for the antitumor effect of mGPD.

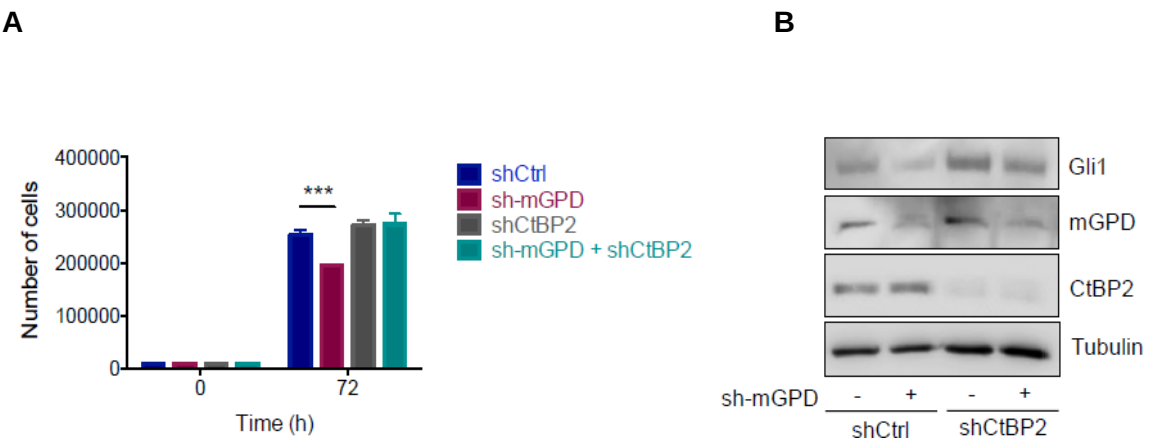

Figure 20. A, Cell proliferation assay in Med1-MB cells stably transduced with lentiviruses expressing control (shCtrl), mGPD, CtBP2-specific shRNAs alone, or in combination for 72 hours. **B**, Gli1, mGPD, CtBP2 protein levels from Med1-MB cells transduced as above were analyzed by western blot at the end of the experiment. Tubulin was used as loading control.

To evaluate the pathophysiological relevance of this mechanism, we studied the phenformin response in CtBP2-deficient tumors. We transduced Med-1 cells with lentiviruses expressing shCtBP2 or shControl shRNAs and preliminarily tested their response to the biguanide *in vitro*. As shown in Figure 21A, 21B 21C phenformin failed to suppress tumor cell growth and Gli1 expression in cells lacking CtBP2.

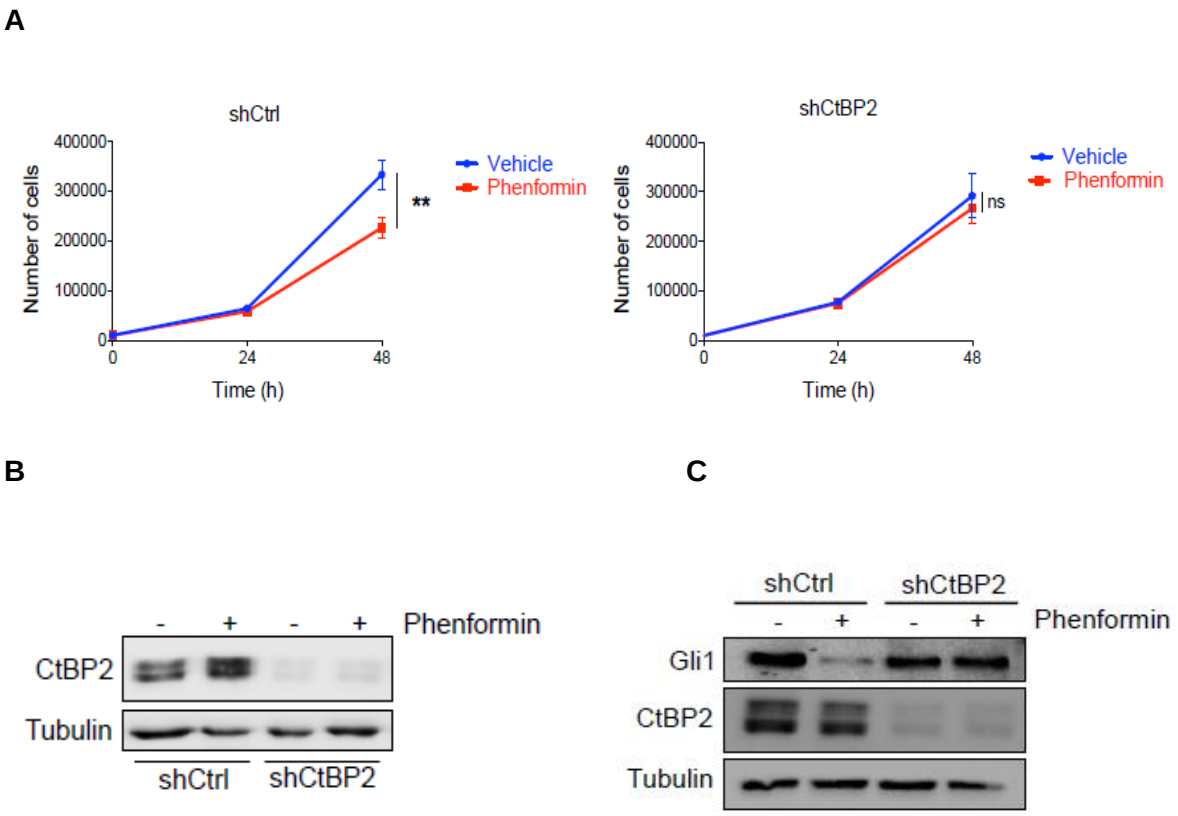

Figure 21. A, Growth curves of Med1-MB cells expressing control (shCtrl) or shCtBP2 and treated with vehicle (DMEM) or phenformin for the indicated time points. **B**, CtBP2 protein levels from Med1-MB cells expressing sh-Control (shCtrl) or CtBP2-specific shRNAs from Figure 21A. Tubulin was used as loading control. **C**, Med1-MB cells stably expressing shControl (shCtrl) or CtBP2-specific shRNAs were treated for 48 hours with vehicle (DMEM) or 5μM phenformin. Lysates were immunobotted with the indicated antibodies.

We then grafted CNBP-deficient or control SHH MB cells into immunodeficient nude mice until the tumor volumes reached 100 mm^3. Mice were divided in two groups: one was treated with 300mg/Kg/day *per os* and the other group was left untreated. As shown in Figure 22A, 22B, the growth rate, the tumor volumes and weights measured at the end of the treatment were significantly reduced by phenformin in control Shh MB, but were not affected by the drug in CtBP2-deficient tumors.

A

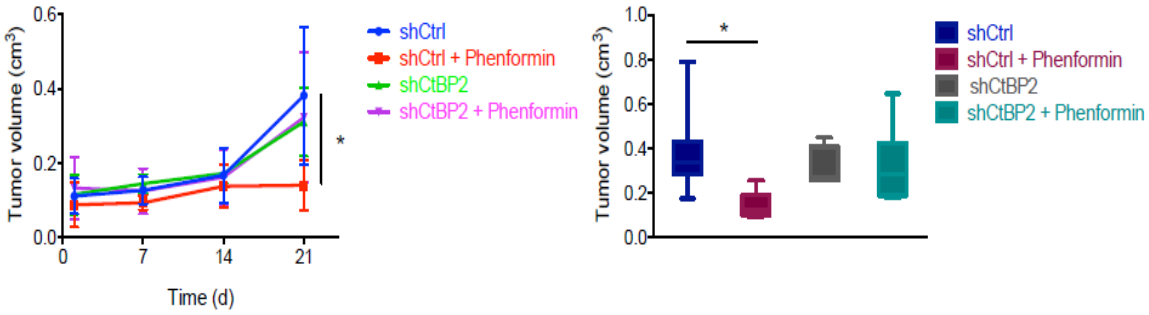

B

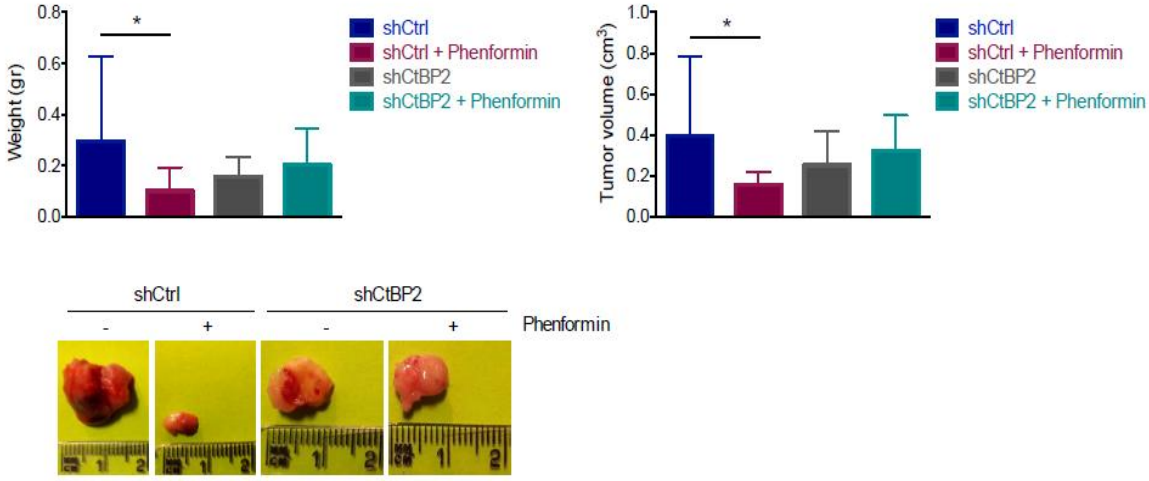

Figure 22. Med1-MB cells were transduced with a lentivirus expressing shControl (shCtrl) or shCtBP2 and injected into the flanks of NOD/SCID mice, which were randomely divided and treated with vehicle (water) or phenformin (300mg/kg/day) through their drinking water. **A**, Left, measurements of tumor volumes on shControl (shCtrl) or shCtBP2 allograft treated with phenformin (300mg/kg/day). n=5 mice per treatment group. (right) Box plots representing the mean tumor burden following 4 weeks of treatment. **B**, Tumor size measurements. Mice were sacrificed after 4 weeks of treatment and allografted tumors were collected for weight (left) and volume (right) measurements. (bottom) Images of excised flank allografts from the treatment groups

Similarly, Gli1 protein and mRNA, as well as Ki67 levels (Figure 23 A, 23 B), were reduced by phenformin in control tumors but were unchanged in samples lacking CtBP2. These latter observations demonstrated the requirement of the redox sensor CtBP2 in mediating the antitumor effect of phenformin on Shh MB growth *in vitro* and *in vivo*.

A

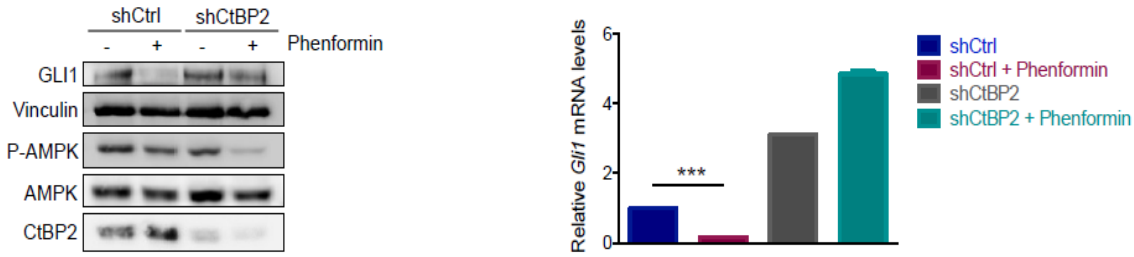

B

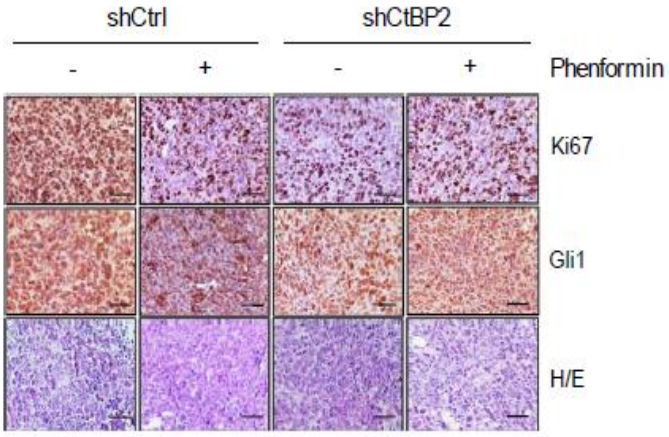

Figure 23. A, Lysates from the tumor allografts described above, were immunoblotted with the indicated antibodies (left) and *Gli1* mRNA levels were analyzed by qPCR (right). **B,** Immunohistochemical analysis of representative allograft tumors stained with the indicated antibodies or H&E. Scale bar = 70 μm.

Taken together, these data demonstrated that the Gli1-CtBP2 complex formation, induced by mGPD-mediated increase of NADH, is a key event underlying the inhibitory effect of phenformin on Hh signaling and tumor growth (Figure 24 A).

A

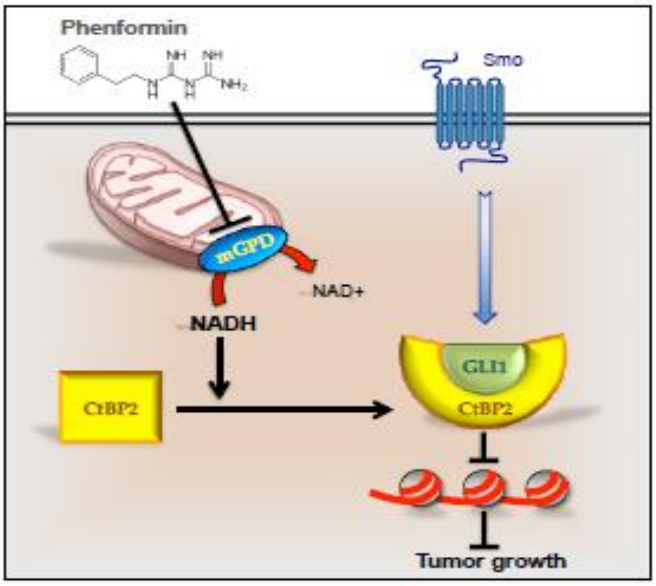

Figure 24. A, Model of the mGPD-CtBP2 mediated phenformin effect on tumor growth. Phenformin treatment inhibits mGPD, causing an increase of cellular NADH. The altered redox state promotes an association between CtBP2 and Gli1, thus inhibiting Hh target gene expression and tumor growth.

All data are represented as the mean ± SD of three independent experiments, each performed in triplicate. **p < 0.01, ***p < 0.001, ns = not significant by ANOVA and unpaired t-test.

DISCUSSION

Driver mutations affecting the Hh signaling are among the 12 key pathway alterations that confer growth advantage to cancer cells (Vogelstein et al., 2013). For this reason, the identification of effective Hh inhibitors represents a relevant achievement in cancer research.

In this work we have demonstrated that tumors characterized by the inappropriate activation of Hh pathway are markedly vulnerable to phenformin, a drug well known for its antitumor properties in several malignancies, whose mechanism of action remains unclear.

A critical and controversial aspect in this regard has been selecting a dose range of phenformin that corresponds to the therapeutic concentration. Based on previous observations in patients, mice, and in our own analyses, we have established that 1-5 micromolar is the appropriate concentration range to achieve therapeutic benefit. Circulating levels beyond these values were not tolerated by our animal models and, to our knowledge, have not been detected in mice or patients. Another important parameter that we have carefully evaluated here is blood glucose concentrations, which were maintained within the physiological range, encompassing circulating values to those within the tumor microenvironment.

Under these conditions, we have found that phenformin displays a significant antitumor effect *in vitro* and *in vivo* on Shh-driven tumor cells that is both independent of the respiratory complex I and perturbations in energy balance, as witnessed by the unmodified OCR and ATP levels, as well as the activities of AMPK, mTOR and adenylyl cyclase.

Conversely, we have shown that the key event underlying the phenformin-dependent tumor properties in Shh MB is the mGPD-mediated increase of the redox state, leading to an elevation of NADH levels. These results support the previous findings by Madiraju et al., who showed that at therapeutic doses biguanides inhibit the glycerophosphate shuttle

in the liver, resulting in an accumulation of lactate and inhibition of hepatic gluconeogenesis without any changes in the energy balance or oxygen consumption (Madiraju et al., 2014).

mGPD catalyzes the oxidation of glycerol-3-phosphate (G3P) to dihydroxyacetone phosphate (DHAP) and the parallel reduction of FAD+ to $FADH_2$. DHAP is in turn reduced to G3P at the expense of NADH oxidation to NAD+ by the cytosolic cGPD enzyme. Both cGPD and mGPD are part of a coupled mechanism in charge of transferring reducing equivalents form the cytosol to the mitochondria, being NADH impermeable to the mitochondrial membrane. The function of the hepatic GPD shuttle appears of particular relevance during the hypoglycemic states, when the body relies mostly on gluconeogenesis to maintain proper blood glucose levels. Under these conditions, or when insulin resistance is encountered, such as in diabetes, the release of TG from the fat tissues is increased and TG are de-esterified in the liver to release G3P, which is then oxidized into DHAP, a key intermediate of gluconeogenesis. Thus, the availability of G3P from TG represents a key determinant for GPD-mediated hepatic gluconeogenesis, a process inhibited by therapeutic doses of biguanides with consequent accumulation of lactate and cytoplasmic NADH (Petersen et al., 2017).

Our observations indicate that inhibition of mGPD in tumor cells leads to the same alterations observed in hepatocytes, suggesting that Shh MB cells may also have elevated levels of G3P available for oxidation. In this regard, a previous work has shown elevated content of TG in Shh MB cells as a consequence of an E2F1-mediated induction of FASN (Bhatia et al., 2011). This observation would be consistent with an increased availability of G3P in these cells and the increase of its mGPD-mediated oxidation to DHAP, a process inhibited by phenformin with consequent NADH accumulation. Since DAHP is also generated from glucose metabolism, and an accumulation of DHAP would reduce G3P oxidation, this metabolic scenario supports the observation that phenformin displays higher efficacy when glucose concentrations are low, evidence also reported by other authors (Birsoy et al., 2014).

A central finding of this report is that the antitumor effect of phenformin is linked to the elevation of the redox state and not to inhibition of respiration and energy balance. A key player of this mechanism is the CtBP2 co-repressor, which responds to the raise of NADH with an increase of the binding with Gli1, leading to transcriptional inhibition of Hh target genes.

CtBP1 and CtBP2 are conserved transcriptional corepressors involved in developmental processes that act as redox sensors through their NADH-binding domain (Chinnadurai, 2002). Upon binding to NADH, CtBPs undergo a conformational change that promotes the associations to their binding partners, which usually occurs through a PXDLS motif of many transcriptional regulators, thereby inhibiting their function (Kumar et al., 2002; Zhang et al., 2002; Zhang et al., 2000). Some proteins, such as HDAC1/2 and LSD1, can interact with CtBPs independently of this sequence, suggesting the involvement of alternative association interfaces or indirect binding (Blevins et al., 2017). Since Gli1 does not have a conserved PXDLS motif, it is possible that the interaction of Gli1 with CtBP2 could also be mediated by other interfaces or by HDAC1/2, which have been found associated to Gli1 (Canettieri et al., 2010).

Interestingly, CtBPs seem to play a context-dependent role in cancer by either supporting or inhibiting tumorigenesis. Indeed, in some tumors, such as prostate cancer and melanoma, CtBP has been described as a tumor suppressor, whereas in several other tumors CtBPs have been found upregulated or associated to pro-tumorigenic functions (Blevins et al., 2017).

In this study we have observed that CtBP2 acts as a suppressor of tumor growth in Shh MB by associating with Gli1 and limiting its transcriptional activity. It is important to note, in this regard, that this inhibitory function is promoted by treatment of cells with therapeutic doses of phenformin, a condition where the redox state seems to be uncoupled from the energy state.

This observation appears to be relevant since studies addressing the function of CtBP as a redox sensor have been performed using drugs or conditions that affect both redox and

energy states, such as hypoxia or 2-Deoxyglucose (2DG) (Shen et al., 2017; Zhang et al., 2006). Our findings that either phenformin treatment or mGPD knockdown have the ability to perturb only the redox state would indicate that further studies should be carried out to address the function of CtBPs under these selective conditions, without altering other unrelated metabolic-driven mechanisms that also have a profound impact on cancer cells. It is likely that in addition to Shh MBs, also in other phenformin-sensitive tumors, CtBPs might exert their antitumor effects by associating with proteins that affect tumorigenesis upon redox-induced conformational change. A study of the CtBP-binding partners under conditions of increased redox state (e.g. phenformin treatment or mGPD ablation) will help to clarify this interesting aspect.

Finally, our data show the significant preclinical efficacy of phenformin on Shh MB through inhibition of Gli1. Of note, phenformin displays its Hh inhibitory effect independently of Smo, as shown by the ability to suppress Hh target gene expression in SuFu-deficient MB cells. This aspect is important since it would imply that a drug already tested in patients acts by inhibiting Hh signaling at a post receptor level and could thus be a potential new weapon against Hh dependent tumors that are or become resistant to Smo inhibitors.

Phenformin has shown stronger anticancer properties compared to metfomin in most of the tumors studied, likely due to its higher hydrophobicity and ability to cross the cell membranes (Janzer et al., 2014). The more elevated permeability is also believed to be the reason of the higher risk of lactic acidosis, which represents the main concern about the use of this drug. However, the remarkable inhibitory effects observed in different type of cancers, and the higher efficacy compared to metformin, have generated the interest to reconsider the use of phenformin with cancer patients, pending appropriate trials to carefully establish the doses that are both safe and effective. A phase Ib clinical trial of a combination of phenformin with BRAF inhibitors in patients with metastatic melanoma (Clincaltrials.gov Identifier NCT03026517) has recently started and will provide critical information in this regard. Whether phenformin will also be a resource for Shh MB patients

thus represents a major issue generated by this work, which deserves further investigation.

MATERIALS AND METHODS

Cell lines and cultures

Med1-MB cells, generated from a spontaneous tumor from Ptch$^{+/-}$;lacZ mouse, were kindly provided by Yoon-Jae Cho (Stanford, CA USA) and cultured in Dulbecco's modified Eagle medium (DMEM) supplemented with 10% FBS, 1mM penicillin-streptomycin and 1mM glutamine. MB cultures were derived from spontaneous, intracranial MB from Math1-Cre/Ptc1$^{fl/fl}$ mice. Tumors were harvested, dissociated and cultured as previously described (Di Magno et al., 2014). DAOY cells were obtained from ATCC and cultured as previously described (Coni et al., 2017; D'Amico et al., 2015; Di Magno et al., 2016). For SAG treatment, DAOY cells were incubated overnight in serum-free medium containing 0.5% BSA and glucose 0.75mM and the exposed to SAG (200nM, #AG-Cr1-3506, Adipogenes Life Sciences) for 48 hours. Phenformin (#P7045), metformin (#D150959) and rotenone (#R8875) were purchased from Sigma-Aldrich, mitochondrial GPDH inhibitor iGP-1 (#530655) was purchased from Calbiochem and dissolved in DMSO. Treatments were performed in DMEM no glucose, no sodium pyruvate (#11966025, Gibco) supplemented with 10% FBS, 1mM penicillin-streptomycin, 1mM glutamine and glucose (25mM or 5.5mM or 0.75mM, as indicated in the text).

Transfections and luciferase assays

Med1-MB cells were transfected with Lipofectamine 2000 (3 µl/µg of DNA, #11668019, Invitrogen) in OptiMem medium (#31985070, Invitrogen). For luciferase assays, Med1-MB cells were seeded and transfected with siRNA against Gli1 (100nM, #M-047917-01, Dharmacon) using Lipofectamine 2000 for 48 hours. After siRNA transfection, cells were re-seeded in 12-well plates and transfected with the 12xGli-Luc luciferase reporter (50ng),

TK-renilla plasmid (10ng) and Flag-CtBP2 or Flag-pcDNA3 (440 ng) expression vectors, using Lipofectamine 2000 for 48 hours. Luciferase reporter assay was performed with the Firefly and Renilla Dual Luciferase Assay kit (#300811, Biotium). Relative luciferase activity is expressed as the ratio of luciferase and renilla activity in control and Gli1 knockdown cells expressing Flag-CtBP2 or Flag-pcDNA3 plasmids.

In vivo mouse studies

Math1-CRE; Ptch1$^{loxP/loxP}$ mice were previously described (Yang et al., 2008). C57BL/6 mice were obtained from The Jackson Laboratory (Bar Harbor, ME, USA). CD1-nude mice and NOD/SCID mice were purchased from Charles Rives Laboratories (Calco, LE, Italy).

For the Kaplan Meier analysis (Figure 4B), Math1-CRE; Ptch1$^{loxP/loxP}$ mice were divided into two treatment groups (n=8): 1) non treated control group and 2) group treated with phenformin at a concentration of 300mg/Kg/day, administered through the drinking water (Appleyard et al., 2012). The treatment started when mice where 35 days old. The survival rate over time was estimated as the number of life days from the start of pharmacological treatment. For short-term treatments (Figure 3B, Figure 12A, scheme in Figure 3A), mice were injected with saline (0.9%) or phenformin and were euthanized at 30 minutes and 1 hour post-injection. Long-term treatments consisted of 10 days (Figure 3C, 3A) to four weeks (Figure 4A, Figure 12B and Figure 22,23) treatment with ad libitum phenformin (300mg/Kg/day).

Tumor allograft experiments were performed as previously described (Di Magno et al., 2014). Four weeks old female NOD/SCID and CD1-nude mice were injected on each flank with 2×10^6 medulloblastoma cells deriving from Math1-CRE; Ptch1$^{loxP/loxP}$ mice, or with 2×10^6 Med1-MB cells stably expressing shRNA-Control or shRNA-CtBP2. Tumors were grown until they reached 100 mm^3 volume. Animals were divided into two groups (n=5)

and administered with vehicle (water) or phenformin (300 mg/Kg/day) in the drinking water (Appleyard et al., 2012). Tumor volumes were measured with a caliper, using the following formula: $V = (L \times W^2)/2$ (Kim et al., 2013). All animal experiments were approved by local ethics authorities.

Determination of cell proliferation and tumorspheres size

2×10^4 Med1-MB cells were seeded in 12-well plate and incubated overnight at 37°C. After 24 hours from seeding, cells were treated with phenformin or metformin at the concentrations indicated in the text. Every 24 hours cells were trypsinized and counted by trypan blue exclusion method.

Tumorspheres diameters were measured using ImageJ software. Briefly, tumorspheres were seeded in Neurobasal-A medium no Glucose (#11966025, Gibco) supplemented with B27 supplement minus vitamin A (#12587010, Gibco), 1mM penicillin-streptomycin, 1mM glutamine and 0.75mM glucose and treated with phenformin (5μM) for 48 hours. After incubation, tumorspheres images were captured under an inverted microscope and diameters were measured.

Western blotting and immunoprecipitation assays

Cells or tissues were collected at the end of the treatments and lysed in denaturing buffer containing 50 mM Tris-HCl, 2% SDS, 10% Glycerol, 10 mM Na4P2O7, 100 mM NaF, 6 M Urea, 10 mM EDTA. Protein extracts were quantified and resolved by SDS–polyacrylamide gel electrophoresis and transferred to a nitrocellulose membrane (#NBA085C001EA, Perkin Elmer). After blocking, membranes were incubated with

primary antibodies overnight and HPR-conjugated secondary antibodies. Detection of the horseradish peroxidase signal was performed using WesternBright ECL (#K-12045-D50), according to the manufacturer's protocol. Immunoprecipitation assays were performed as previously described (Canettieri et al., 2010).

Plasmids and antibodies

HA-CtBP1 plasmid was a gift from Dr. Ulupi Jhala (PDRC, CA USA). Flag-Myc-CtBP2 was purchased from Origene (#TP324861). 12xGli-Luc, TK-renilla, Flag-pcDNA3, Myc-GLI2 and Flag-GLI3 were previously described (Canettieri et al., 2009; Canettieri et al., 2010). The following antibodies were used: Gli1 (#2643S Cell Signaling, WB 1:1000), AMPK (#2532S Cell Signaling WB 1:1000), phospho-AMPK (#2535S Cell Signaling, WB 1:1000), CtBP2 (#13256S Cell Signaling, WB 1:1000), CtBP2 (#612044 BD Biosciences, ChIP 1:1000), GPD2 (D12) (#sc-390830 SantaCruz Biotechnology, WB 1:500), Flag-HRP (#A8592 Sigma-Aldrich, WB 1:10000), HA-HRP (#H6533 Sigma-Aldrich, WB 1:10000), Tubulin (#sc-8035 SantaCruz Biotechnology, WB 1:1000), Vinculin (#sc-73614 SantaCruz Biotechnology, WB 1:1000), Ki67 (#MA5-14520 Pierce, IHC 1:100), phospho-4EBP1 (#9456S Cell Signaling, WB 1:1000), 4EBP1 (#9644 Cell Signaling, WB 1:1000), phospho-CREB (from Dr. Marc Montminy's laboratory, Salk Institute, WB 1:2000), Cyclin D1 (#sc-717 SantaCruz Biotechnology, WB 1:1000), Cyclin A (#sc-751 SantaCruz Biotechnology, WB 1:1000), Cyclin E (#sc-25303 SantaCruz Biotechnology, WB 1:1000), p21 (#sc-817 SantaCruz Biotechnology, WB 1:1000), SuFu (#2522S Cell Signaling, WB 1:1000), Actin (#sc-8432 SantaCruz Biotechnology, WB 1:1000), Gli1 (H300) (#sc-20687 SantaCruz Biotechnology, IHC 1:200), phospho-ACC (#sc-20687 SantaCruz Biotechnology, WB 1:1000), Myc-HRP (#sc-20687 SantaCruz Biotechnology, WB 1:5000).

Lentiviral-mediated shRNA knockdown

shRNA knockdown was performed through lentiviral infection. HEK293 cells were transfected by calcium phosphate precipitation with 20 µg of different pLKO.1 vectors (Sigma-Aldrich) together with 15 µg of pCMV-R 8.74, and 10 µg of pMD.G, to produce lentiviruses. After 24 hours, the medium was changed and supernatant containing recombinant lentiviruses was collected 48 and 72 hours after transfection. AMPKα1 (TRCN0000360841), SuFu (TRCN0000019464) and control shRNA (scrambled shc002) were obtained by Sigma-Aldrich. PLKO.1 vector expressing shRNA directed against, AMPKα2, cGPD, mGPD and CtBP2 were cloned in PLKO.1 TCR vector with the oligos listed below. Virus titers were determined using quantitative real-time PCR as previously described (Barczak et al., 2015). To perform lentiviral transduction, Med1-MB cells were seeded overnight in 60mm plates. The day after, 5 MOI of lentivirus were complexed with 5 µg/ml polybrene, added to the cells and left 24 hours before being removed and replaced with standard medium. Knockdown efficiency was monitored by western blotting and/or qPCR.

Oligo	Direction	Sequence
shAMPKα2	Forward	CCGGTATTATCTCACTCGGTATTACTCTAGAGTAATACCGAGTGAGATA ATATTATTG
	Reverse	AATCAAAAATTATCTCACTCGGTATTACCTCTAGAGTAATACCGAGTGA GATAATATTA
sh-cGPD	Forward	CCGGCCATCAGTTCATTGGCAAGATTCTAGAATCTTGCCAATCTTGCCA ATGAACTGATGGTTTTTG
	Reverse	AATCAAAAACCATCAGTTCATTGGCAAGATTCTAGAATCTTGCCAATCT TGCCAATGAACTGATGG
sh-mGPD	Forward	CCGGGCAGAGGTGAAATACGGCATTTCTAGAAATGCCGTATTTCACCTC TGCTTG
	Reverse	AATCAAAAAGCAGAGGTGAAATACGGCATTTCTAGAAATGCCGTATTTC ACCTCTGC
shCtBP2	Forward	CCGGTACGAAACTGTGTCAACAAAGTCTAGACTTTGTTGACACAGTTTCG TATTATTG
	Reverse	AATCAAAAATACGAAACTGTGTCAACAAAGTCTAGACTTTGTTGACACAG TTTCGTA

Quantitative Real-Time PCR (qPCR) assay

Total mRNA was isolated from cells as previously described (Canettieri et al., 2010). Complementary DNA (cDNA) was synthesized by the Sensifast cDNA synthesis kit (#BIO-65054, Bioline). Quantitative PCR was performed with SensiFast Sybr Lo-Rox Mix (#BIO-94020, Bioline), and transcript levels were quantified with the Applied Biosystems ViiA 7 Real-Time PCR System instrument. Each sample was normalized on *L32* mRNA levels. Primer sequences are listed below.

Gene	Direction	Sequence
L32	Forward	AGAGGTGCTGGGAGCTGCTA
	Reverse	GATGGATGGTCTCTGGACGG
Gli1	Forward	GCCAACTTTATGTCAGGGTCCCAG
	Reverse	GGAGAGAGCCCGCTTCTTTGTTAA
mGPD	Forward	TGCGCGGTGCAAGGAT
	Reverse	GCATTTGGCTCTCACGTCAA
cGPD	Forward	CCTGATGCAGACACCCAACT
	Reverse	AAGCCAAGCCCATCACAGAA
CtBP2	Forward	TTTGTGAAGGTATCCGCCCC
	Reverse	GGTACATCATGGCACCCACA
Ptch1	Forward	GAGCATTCCTTAATGGAAG
	Reverse	CTGCAACGCGATTGGCTCT
Cyclin D2	Forward	AGAAGGACATCCAACCGTACATG
	Reverse	CATGGCCAGAGGAAAGACCTC

Chromatin immunoprecipitation (ChIP) assay

Chromatin immunoprecipitation experiments were performed as described previously (Canettieri et al., 2010). Rabbit polyclonal anti-CtBP2 (#612044, BD Biosciences) antibody was used to precipitate endogenous CtBP2. Eluted DNA was PCR-amplified with primers encompassing the Ptch1 promoter or *Hprt* gene as internal control.

Immunohistochemistry (IHC)

Immunohistochemical analysis of allografted tumor sections was performed as described (Coni et al., 2013). The following antibodies and conditions were used: Ki67 was diluted in PBS-T containing 1% serum, GLI1 (H300) was diluted in PBS-T containing 5% serum.

Antibodies were incubated for one hour at room temperature. Nuclei were counterstained with hematoxylin in accordance with standard procedures.

Determination of phenformin concentration

All chemicals were of analytical grade, readily available commercial products and were obtained from Sigma-Aldrich (San Louis, MO, USA). The HPLC-system was an Agilent Technologies 1200 Series equipped with a variable wavelength detector (VWD) operating at a wavelength of 240 nm. All the operations, such as the injection cycle, were controlled by the ChemStation program; the data obtained were analyzed with the ChemStation program (Agilent Technologies Deutschland GmbH, Waldbronn, Germany). Stock standard solutions of phenformin were prepared by dissolving 10 mg of analyte in 10 mL of water/methanol (50/50) to make a standard solution of 1 mg/mL. Piperacillin internal standard stock solution was prepared by dissolving 10 mg piperacillin in 10 mL of water to obtain a concentration of 1 mg/mL. The stock standards and internal standard solutions were aliquoted (200 µL) and stored at - 80°C until use. Calibration samples of phenformin (30-10000 ng/mL) and internal standard (200 µg/mL) were prepared by adding varying volumes of standard stock solutions and fixed volume of internal standard stock solution into pooled drug-free plasma. The peak area ratio of phenformin to internal standard was measured, and a calibration curve was obtained from the least-squares linear regression of the peak area ratio with spiked concentrations.

The extraction procedure and HPLC analysis has been performed, with changes, as reported by (Cheng and Chou, 2001). Briefly, up to 200 µL of blood samples were collected into a 0.2mL capillary tube and transferred into micro-tubes, both containing sprayed EDTA, and immediately centrifuged. The plasma was stored at -80°C. Tissues sample were collected into 1mL tubes, sonicated and stored at -80°C. Samples were prepared as follows: sample (100 µL) was spiked with 10 µL of the internal standard solution (piperacillin 200 µg/mL) and 10 µL of 1M HCl. After vortexing for 30 seconds, the

mixture was extracted with 300 µL of acetonitrile by vortex for 30 seconds, and then centrifuged at 13,000 rpm for 9 minutes. The organic phase was separated and evaporated to dryness at 30°C and under a nitrogen stream. The extracts were reconstituted with 100 µL of water and washed with 150 µL of dichloromethane by vortex for 30 seconds. After centrifugation at 13,000 rpm for 9 minutes, 60 µL of aqueous layer was injected into a Kinetex Biphenyl LC column (150x4.6 mm; 5 µm particle size; Phenomenex). Phenformin was isocratically eluted from the column using mobile phase acetonitrile:phosphate buffer 30 mM pH 7.0, 25:75, v/v.

Retention time of phenformin was 2.715 minutes at 30°C and a flow rate of 1 mL/min. Total HPLC run time was 5 minutes; re-equilibration time was 0.3 minutes. The concentrations of phenformin were calculated according to the peak area and were compared both with piperacillin as internal standard and with reference curves constructed with escalating concentration of phenformin (30 to 10000 ng/mL).

Metabolic assays

Real time bioenergetics analysis of oxygen consumption rate (OCR) was performed using the XF^e -96 Extracellular Flux Analyzer (Seahorse Bioscience). Cells were seeded at a density of $4x10^3$ cells/well in XF^e-96 plates (Seahorse Bioscience) and cultured in 200µl Dulbecco's modified Eagle's medium containing 25 mM glucose and 1mM glutamine for 24hr and treated with the indicated drugs for 6 hours in DMEM containing 0.75 mM glucose. Wells were washed and cells were incubated in a CO_2-free incubator to allow equilibration prior to loading into the XF-96 apparatus. OCR was measured in XF medium (non-buffered DMEM medium containing 0.75mM glucose and 1mM glutamine). Perturbation profiling of the use of metabolic pathways was achieved using the Seahorse XF Cell Mito Stress Test Kit (#103015-100). The assay conditions in the Seahorse experiments were: 3 min of mixture; 3 min of waiting; and 3 min of measurement.

Total cellular NADH and tissutal NADH were determined using the EnzyChrom NAD+/NADH Assay Kit (#E2ND-100, BioAssay Systems) and following manufacturer's instructions. Briefly, 1 x 10^5 cells or 20 mg of tissue were harvested and homogenized in 100µl NADH extraction buffer. After incubation at 60°C, samples were neutralized adding 100µl NAD extraction buffer and 20µl Assay buffer. Sample were briefly vortexed and spinned down to remove cellular debris. The supernatant was used for NADH measurement with OD at 565 nm using a spectrophotometer. Values were corrected for dilutions and protein content or weight of the samples.

Total cellular ATP and tissue ATP were determined using the CellTiter-Glo® Luminescent Cell Viability Assay (#G7571, Promega). Briefly, Med1-MB cells were seeded into 96-well plates (4 x 10^3 cells per well) and incubated for 24 hours. After incubation, cells were treated with phenformin for 6 hours. For tissue samples, ATP was extracted as previously described (Chida et al., 2012). The luminescence assay was performed according to the manufacturer's instructions.

Analysis of metabolites by GC-MS

Lactic acid and pyruvic acid were analyzed as methoxime/tertbutyldimethylsilyl derivatives as previously described (Paik et al., 2008). Briefly, cells were collected by centrifugation at 1000 rpm for 5 minutes. 20 µL of supernatant were deproteinized by adding 100 µL of acetonitrile and vortexed for 3 minutes. The mixtures were diluted 1:10 with distilled water and centrifuged at 15,000 rpm for 15 minutes at 4°C to pellet proteins. The deproteinized supernatant was used to quantify extracellular L-lactate by GC-SIM-MS analysis. Aliquots of 0.25 mL of the supernatant layer spiked with the internal standard (IS) 3,4-dimethoxybenzoyc acid (final concentration 1000 ng ml^{-1}) were added to 0.7 mL of distilled water and adjusted to pH ≥13 with 7 M NaOH. Methoxymation was performed by adding to the reaction mix methoxyamine hydrochloride (5 mg) at 60°C for 60 min. The

samples were then washed with diethylether (3 mL × 2) and the aqueous phase was adjusted to pH < 2 with concentrated sulfuric acid. The mixture was saturated with NaCl and extracted with diethyl ether (3 ml) and ethyl acetate (2 ml). The organic extracts were combined in the presence of triethylamine (10 µl) and dried under reduced pressure. The samples were then suspended in 30 µl of toluene subjected to the second derivatization step by adding 20 mL of MTBSTFA (65°C for 30 min) and analyzed by GC-MS. Results were normalized on cell number and expressed as fold change relative to control samples.

Cerebellum samples were homogenized in a ice-bath using an ultra-turrax T8 blender with the addition of 1 mL water:acetonitrile (9:1). The homogenized tissue was centrifuged at 13,000 g for 15 minutes at 4°C. 0.25 mL of the cerebellum extract were spiked with internal standard (IS) 3,4-dimethoxybenzoyc acid (final concentration 1000 ng mL^{-1}) and subjected to methoxymation/ tertbutyldimethylsilylation as described above. Results were normalized by tissue weight and expressed as fold change relative to control samples.

GC-M analyses were performed with an Agilent 6850A gas chromatograph coupled to a 5973N quadrupole mass selective detector (Agilent Technologies, Palo Alto, CA, USA). Chromatographic separations were carried out with an Agilent HP5ms fused-silica capillary column (30 m × 0.25 mm i.d.) coated with 5%- phenyl-95%-dimethylpolysiloxane (film thickness 0.25 µm) as stationary phase. Injection mode: splitless at a temperature of 280 °C. Column temperature program: 70 °C (1 min) then to 300 °C at a rate of 20 °C/min and held for 10 min. The carrier gas was helium at a constant flow of 1.0 mL/min. The spectra were obtained in the electron impact mode at 70 eV ionization energy; ion source 280 °C; ion source vacuum 10^{-5} Torr.MS analysis was performed simultaneously in TIC (mass range scan from m/z 50 to 600 at a rate of 0.42 scans s^{-1}) and SIM mode. GC-SIM-MS analysis was performed selecting the following ions: m/z 174 for pyruvate, m/z 261 for lactate and m/z 239 for 3,4-dimethoxybenzoic acid (internal standard).

Statistical analysis

Statistical analysis was performed using Prism software (GraphPad). Data were analyzed with a paired Student's t test, ANOVA or log-rank test and expressed as mean ± SD. $p < 0.05$ was considered statistically significant.

REFERENCES

1. Appleyard, M. V., Murray, K. E., Coates, P. J., Wullschleger, S., Bray, S. E., Kernohan, N. M., Fleming, S., Alessi, D. R., and Thompson, A. M. (2012). Phenformin as prophylaxis and therapy in breast cancer xenografts. Br J Cancer *106*, 1117-1122.
2. Barczak, W., Suchorska, W., Rubis, B., and Kulcenty, K. (2015). Universal real-time PCR-based assay for lentiviral titration. Molecular biotechnology *57*, 195-200.
3. Berger, W. (1985). Incidence of severe sideeffects during therapy with sulfonylureas and biguanides. Hormone and metabolic research Supplement series *15*, 111-115.
4. Bhatia, B., Hsieh, M., Kenney, A. M., and Nahle, Z. (2011). Mitogenic Sonic hedgehog signaling drives E2F1-dependent lipogenesis in progenitor cells and medulloblastoma. Oncogene *30*, 410-422.
5. Birsoy, K., Possemato, R., Lorbeer, F. K., Bayraktar, E. C., Thiru, P., Yucel, B., Wang, T., Chen, W. W., Clish, C. B., and Sabatini, D. M. (2014). Metabolic determinants of cancer cell sensitivity to glucose limitation and biguanides. Nature *508*, 108-112.
6. Blevins, M. A., Huang, M., and Zhao, R. (2017). The Role of CtBP1 in Oncogenic Processes and Its Potential as a Therapeutic Target. Mol Cancer Ther *16*, 981-990.
7. Briscoe, J., and Therond, P. P. (2013). The mechanisms of Hedgehog signalling and its roles in development and disease. Nat Rev Mol Cell Biol *14*, 416-429.
8. Canettieri, G., Coni, S., Della Guardia, M., Nocerino, V., Antonucci, L., Di Magno, L., Screaton, R., Screpanti, I., Giannini, G., and Gulino, A. (2009). The coactivator CRTC1 promotes cell proliferation and transformation via AP-1. Proc Natl Acad Sci U S A *106*, 1445-1450.

9. Canettieri, G., Di Marcotullio, L., Greco, A., Coni, S., Antonucci, L., Infante, P., Pietrosanti, L., De Smaele, E., Ferretti, E., Miele, E.*, et al.* (2010). Histone deacetylase and Cullin3-REN(KCTD11) ubiquitin ligase interplay regulates Hedgehog signalling through Gli acetylation. Nat Cell Biol *12*, 132-142.
10. Che, J., Zhang, F. Z., Zhao, C. Q., Hu, X. D., and Fan, S. J. (2013). Cyclopamine is a novel Hedgehog signaling inhibitor with significant anti-proliferative, anti-invasive and anti-estrogenic potency in human breast cancer cells. Oncology letters *5*, 1417-1421.
11. Cheng, C. L., and Chou, C. H. (2001). Determination of metformin in human plasma by high-performance liquid chromatography with spectrophotometric detection. Journal of chromatography B, Biomedical sciences and applications *762*, 51-58.
12. Chida, J., Yamane, K., Takei, T., and Kido, H. (2012). An efficient extraction method for quantitation of adenosine triphosphate in mammalian tissues and cells. Analytica chimica acta *727*, 8-12.
13. Chinnadurai, G. (2002). CtBP, an unconventional transcriptional corepressor in development and oncogenesis. Mol Cell *9*, 213-224.
14. Coni, S., Antonucci, L., D'Amico, D., Di Magno, L., Infante, P., De Smaele, E., Giannini, G., Di Marcotullio, L., Screpanti, I., Gulino, A., and Canettieri, G. (2013). Gli2 acetylation at lysine 757 regulates hedgehog-dependent transcriptional output by preventing its promoter occupancy. PLoS One *8*, e65718.
15. Coni, S., Mancuso, A. B., Di Magno, L., Sdruscia, G., Manni, S., Serrao, S. M., Rotili, D., Spiombi, E., Bufalieri, F., Petroni, M.*, et al.* (2017). Selective targeting of HDAC1/2 elicits anticancer effects through Gli1 acetylation in preclinical models of SHH Medulloblastoma. Scientific reports *7*, 44079.
16. D'Amico, D., Antonucci, L., Di Magno, L., Coni, S., Sdruscia, G., Macone, A., Miele, E., Infante, P., Di Marcotullio, L., De Smaele, E.*, et al.* (2015). Non-

canonical Hedgehog/AMPK-Mediated Control of Polyamine Metabolism Supports Neuronal and Medulloblastoma Cell Growth. Dev Cell *35*, 21-35.

17. Di Magno, L., Basile, A., Coni, S., Manni, S., Sdruscia, G., D'Amico, D., Antonucci, L., Infante, P., De Smaele, E., Cucchi, D.*, et al.* (2016). The energy sensor AMPK regulates Hedgehog signaling in human cells through a unique Gli1 metabolic checkpoint. Oncotarget *7*, 9538-9549.
18. Di Magno, L., Coni, S., Di Marcotullio, L., and Canettieri, G. (2015). Digging a hole under Hedgehog: downstream inhibition as an emerging anticancer strategy. Biochim Biophys Acta *1856*, 62-72.
19. Di Magno, L., Manzi, D., D'Amico, D., Coni, S., Macone, A., Infante, P., Di Marcotullio, L., De Smaele, E., Ferretti, E., Screpanti, I.*, et al.* (2014). Druggable glycolytic requirement for Hedgehog-dependent neuronal and medulloblastoma growth. Cell Cycle *13*, 3404-3413.
20. Dykens, J. A., Jamieson, J., Marroquin, L., Nadanaciva, S., Billis, P. A., and Will, Y. (2008). Biguanide-induced mitochondrial dysfunction yields increased lactate production and cytotoxicity of aerobically-poised HepG2 cells and human hepatocytes in vitro. Toxicology and applied pharmacology *233*, 203-210.
21. El-Mir, M. Y., Nogueira, V., Fontaine, E., Averet, N., Rigoulet, M., and Leverve, X. (2000). Dimethylbiguanide inhibits cell respiration via an indirect effect targeted on the respiratory chain complex I. J Biol Chem *275*, 223-228.
22. Foretz, M., Guigas, B., Bertrand, L., Pollak, M., and Viollet, B. (2014). Metformin: From Mechanisms of Action to Therapies. Cell Metabolism *20*, 953-966.
23. Foretz, M., Hebrard, S., Leclerc, J., Zarrinpashneh, E., Soty, M., Mithieux, G., Sakamoto, K., Andreelli, F., and Viollet, B. (2010). Metformin inhibits hepatic gluconeogenesis in mice independently of the LKB1/AMPK pathway via a decrease in hepatic energy state. J Clin Invest *120*, 2355-2369.

24. Goodrich, L. V., Milenkovic, L., Higgins, K. M., and Scott, M. P. (1997). Altered neural cell fates and medulloblastoma in mouse patched mutants. Science *277*, 1109-1113.
25. Gotschel, F., Berg, D., Gruber, W., Bender, C., Eberl, M., Friedel, M., Sonntag, J., Rungeler, E., Hache, H., Wierling, C.*, et al.* (2013). Synergism between Hedgehog-GLI and EGFR signaling in Hedgehog-responsive human medulloblastoma cells induces downregulation of canonical Hedgehog-target genes and stabilized expression of GLI1. PLoS One *8*, e65403.
26. Gruber, W., Peer, E., Elmer, D. P., Sternberg, C., Tesanovic, S., Del Burgo, P., Coni, S., Canettieri, G., Neureiter, D., Bartz, R.*, et al.* (2018). Targeting class I histone deacetylases by the novel small molecule inhibitor 4SC-202 blocks oncogenic hedgehog-GLI signaling and overcomes smoothened inhibitor resistance. International journal of cancer Journal international du cancer *142*, 968-975.
27. Hayden Gephart, M. G., Su, Y. S., Bandara, S., Tsai, F. C., Hong, J., Conley, N., Rayburn, H., Milenkovic, L., Meyer, T., and Scott, M. P. (2013). Neuropilin-2 contributes to tumorigenicity in a mouse model of Hedgehog pathway medulloblastoma. J Neurooncol *115*, 161-168.
28. He, L., and Wondisford, F. E. (2015). Metformin action: concentrations matter. Cell Metab *21*, 159-162.
29. Huang, X., Wullschleger, S., Shpiro, N., McGuire, V. A., Sakamoto, K., Woods, Y. L., McBurnie, W., Fleming, S., and Alessi, D. R. (2008). Important role of the LKB1-AMPK pathway in suppressing tumorigenesis in PTEN-deficient mice. The Biochemical journal *412*, 211-221.
30. Infante, P., Alfonsi, R., Botta, B., Mori, M., and Di Marcotullio, L. (2015). Targeting GLI factors to inhibit the Hedgehog pathway. Trends Pharmacol Sci *36*, 547-558.
31. Jackson, A. L., Sun, W., Kilgore, J., Guo, H., Fang, Z., Yin, Y., Jones, H. M., Gilliam, T. P., Zhou, C., and Bae-Jump, V. L. (2017). Phenformin has anti-

tumorigenic effects in human ovarian cancer cells and in an orthotopic mouse model of serous ovarian cancer. Oncotarget *8*, 100113-100127.

32. Janzer, A., German, N. J., Gonzalez-Herrera, K. N., Asara, J. M., Haigis, M. C., and Struhl, K. (2014). Metformin and phenformin deplete tricarboxylic acid cycle and glycolytic intermediates during cell transformation and NTPs in cancer stem cells. Proc Natl Acad Sci U S A *111*, 10574-10579.
33. Kalender, A., Selvaraj, A., Kim, S. Y., Gulati, P., Brule, S., Viollet, B., Kemp, B. E., Bardeesy, N., Dennis, P., Schlager, J. J.*, et al.* (2010). Metformin, independent of AMPK, inhibits mTORC1 in a rag GTPase-dependent manner. Cell Metab *11*, 390-401.
34. Kenney, A. M., and Rowitch, D. H. (2000). Sonic hedgehog promotes G(1) cyclin expression and sustained cell cycle progression in mammalian neuronal precursors. Mol Cell Biol *20*, 9055-9067.
35. Kim, J., Aftab, B. T., Tang, J. Y., Kim, D., Lee, A. H., Rezaee, M., Kim, J., Chen, B., King, E. M., Borodovsky, A.*, et al.* (2013). Itraconazole and arsenic trioxide inhibit Hedgehog pathway activation and tumor growth associated with acquired resistance to smoothened antagonists. Cancer Cell *23*, 23-34.
36. Kumar, V., Carlson, J. E., Ohgi, K. A., Edwards, T. A., Rose, D. W., Escalante, C. R., Rosenfeld, M. G., and Aggarwal, A. K. (2002). Transcription corepressor CtBP is an NAD(+)-regulated dehydrogenase. Mol Cell *10*, 857-869.
37. Li, Y. H., Luo, J., Mosley, Y. C., Hedrick, V. E., Paul, L. N., Chang, J., Zhang, G., Wang, Y. K., Banko, M. R., Brunet, A.*, et al.* (2015). AMP-Activated Protein Kinase Directly Phosphorylates and Destabilizes Hedgehog Pathway Transcription Factor GLI1 in Medulloblastoma. Cell reports.
38. Madiraju, A. K., Erion, D. M., Rahimi, Y., Zhang, X. M., Braddock, D. T., Albright, R. A., Prigaro, B. J., Wood, J. L., Bhanot, S., MacDonald, M. J.*, et al.* (2014). Metformin suppresses gluconeogenesis by inhibiting mitochondrial glycerophosphate dehydrogenase. Nature *510*, 542-546.

39. Miller, R. A., Chu, Q., Xie, J., Foretz, M., Viollet, B., and Birnbaum, M. J. (2013). Biguanides suppress hepatic glucagon signalling by decreasing production of cyclic AMP. Nature *494*, 256-260.
40. Nattrass, M., Sizer, K., and Alberti, K. G. (1980). Correlation of plasma phenformin concentration with metabolic effects in normal subjects. Clin Sci (Lond) *58*, 153-155.
41. Orr, A. L., Ashok, D., Sarantos, M. R., Ng, R., Shi, T., Gerencser, A. A., Hughes, R. E., and Brand, M. D. (2014). Novel inhibitors of mitochondrial sn-glycerol 3-phosphate dehydrogenase. PLoS One *9*, e89938.
42. Owen, M. R., Doran, E., and Halestrap, A. P. (2000). Evidence that metformin exerts its anti-diabetic effects through inhibition of complex 1 of the mitochondrial respiratory chain. Biochemical Journal *348*, 607-614.
43. Paik, M. J., Cho, E. Y., Kim, H., Kim, K. R., Choi, S., Ahn, Y. H., and Lee, G. (2008). Simultaneous clinical monitoring of lactic acid, pyruvic acid and ketone bodies in plasma as methoxime/tert-butyldimethylsilyl derivatives by gas chromatography-mass spectrometry in selected ion monitoring mode. Biomedical chromatography : BMC *22*, 450-453.
44. Petersen, M. C., Vatner, D. F., and Shulman, G. I. (2017). Regulation of hepatic glucose metabolism in health and disease. Nature reviews Endocrinology *13*, 572-587.
45. Plaisant, M., Giorgetti-Peraldi, S., Gabrielson, M., Loubat, A., Dani, C., and Peraldi, P. (2011). Inhibition of hedgehog signaling decreases proliferation and clonogenicity of human mesenchymal stem cells. PLoS One *6*, e16798.
46. Pollak, M. (2013). Potential applications for biguanides in oncology. J Clin Invest *123*, 3693-3700.
47. Rosilio, C., Lounnas, N., Nebout, M., Imbert, V., Hagenbeek, T., Spits, H., Asnafi, V., Pontier-Bres, R., Reverso, J., Michiels, J. F.*, et al.* (2013). The metabolic perturbators metformin, phenformin and AICAR interfere with the growth and

survival of murine PTEN-deficient T cell lymphomas and human T-ALL/T-LL cancer cells. Cancer letters *336*, 114-126.

48. Segal, E. D., Yasmeen, A., Beauchamp, M. C., Rosenblatt, J., Pollak, M., and Gotlieb, W. H. (2011). Relevance of the OCT1 transporter to the antineoplastic effect of biguanides. Biochem Biophys Res Commun *414*, 694-699.
49. Shackelford, D. B., Abt, E., Gerken, L., Vasquez, D. S., Seki, A., Leblanc, M., Wei, L., Fishbein, M. C., Czernin, J., Mischel, P. S., and Shaw, R. J. (2013). LKB1 inactivation dictates therapeutic response of non-small cell lung cancer to the metabolism drug phenformin. Cancer Cell *23*, 143-158.
50. Shaw, R. J. (2009). LKB1 and AMP-activated protein kinase control of mTOR signalling and growth. Acta physiologica *196*, 65-80.
51. Shaw, R. J., Lamia, K. A., Vasquez, D., Koo, S. H., Bardeesy, N., Depinho, R. A., Montminy, M., and Cantley, L. C. (2005). The kinase LKB1 mediates glucose homeostasis in liver and therapeutic effects of metformin. Science *310*, 1642-1646.
52. Shen, Y., Kapfhamer, D., Minnella, A. M., Kim, J. E., Won, S. J., Chen, Y., Huang, Y., Low, L. H., Massa, S. M., and Swanson, R. A. (2017). Bioenergetic state regulates innate inflammatory responses through the transcriptional co-repressor CtBP. Nature communications *8*, 624.
53. Steven, A., and Seliger, B. (2016). Control of CREB expression in tumors: from molecular mechanisms and signal transduction pathways to therapeutic target. Oncotarget *7*, 35454-35465.
54. Tang, Y., Gholamin, S., Schubert, S., Willardson, M. I., Lee, A., Bandopadhayay, P., Bergthold, G., Masoud, S., Nguyen, B., Vue, N.*, et al.* (2014). Epigenetic targeting of Hedgehog pathway transcriptional output through BET bromodomain inhibition. Nat Med *20*, 732-740.
55. Vogelstein, B., Papadopoulos, N., Velculescu, V. E., Zhou, S., Diaz, L. A., Jr., and Kinzler, K. W. (2013). Cancer genome landscapes. Science *339*, 1546-1558.

56. Wang, Y., Ding, Q., Yen, C. J., Xia, W., Izzo, J. G., Lang, J. Y., Li, C. W., Hsu, J. L., Miller, S. A., Wang, X.*, et al.* (2012). The crosstalk of mTOR/S6K1 and Hedgehog pathways. Cancer Cell *21*, 374-387.
57. Yang, Z. J., Ellis, T., Markant, S. L., Read, T. A., Kessler, J. D., Bourboulas, M., Schuller, U., Machold, R., Fishell, G., Rowitch, D. H.*, et al.* (2008). Medulloblastoma can be initiated by deletion of Patched in lineage-restricted progenitors or stem cells. Cancer Cell *14*, 135-145.
58. Zhang, Q., Piston, D. W., and Goodman, R. H. (2002). Regulation of corepressor function by nuclear NADH. Science *295*, 1895-1897.
59. Zhang, Q., Wang, S. Y., Nottke, A. C., Rocheleau, J. V., Piston, D. W., and Goodman, R. H. (2006). Redox sensor CtBP mediates hypoxia-induced tumor cell migration. Proc Natl Acad Sci U S A *103*, 9029-9033.
60. Zhang, Q., Yao, H., Vo, N., and Goodman, R. H. (2000). Acetylation of adenovirus E1A regulates binding of the transcriptional corepressor CtBP. Proc Natl Acad Sci U S A *97*, 14323-14328.
61. Zhou, G., Myers, R., Li, Y., Chen, Y., Shen, X., Fenyk-Melody, J., Wu, M., Ventre, J., Doebber, T., Fujii, N.*, et al.* (2001). Role of AMP-activated protein kinase in mechanism of metformin action. J Clin Invest *108*, 1167-1174.